nature
REVIEWS
April 2017 volume 2 no. 4
www.nature.com/reviews

MATERIALS

Printing, folding and assembly methods for forming 3D mesostructures in advanced materials

Yihui Zhang[1], Fan Zhang[1], Zheng Yan[2], Qiang Ma[1], Xiuling Li[3], Yonggang Huang[4] and John A. Rogers[5]

Abstract | A rapidly expanding area of research in materials science involves the development of routes to complex 3D structures with feature sizes in the mesoscopic range (that is, between tens of nanometres and hundreds of micrometres). A goal is to establish methods for controlling the properties of materials systems and the function of devices constructed with them, not only through chemistry and morphology, but also through 3D architectures. The resulting systems, sometimes referred to as metamaterials, offer engineered behaviours with optical, thermal, acoustic, mechanical and electronic properties that do not occur in the natural world. Impressive advances in 3D printing techniques represent some of the most broadly recognized developments in this field, but recent successes with strategies based on concepts in origami, kirigami and deterministic assembly provide additional, unique options in 3D design and high-performance materials. In this Review, we highlight the latest progress and trends in methods for fabricating 3D mesostructures, beginning with the development of advanced material inks for nozzle-based approaches to 3D printing and new schemes for 3D optical patterning. In subsequent sections, we summarize more recent methods based on folding, rolling and mechanical assembly, including their application with materials such as designer hydrogels, monocrystalline inorganic semiconductors and graphene.

[1]*Center for Mechanics and Materials, AML, Department of Engineering Mechanics, Tsinghua University, Beijing 100084, China.*
[5]*Departments of Materials Science and Engineering, Biomedical Engineering, Neurological Surgery, Chemistry, Mechanical Engineering, Electrical Engineering and Computer Science; Center for Bio-Integrated Electronics; and Simpson Querrey Institute for BioNanotechnology, Northwestern University, Evanston, Illinois 60208, USA.*

Correspondence to Y.Z. and J.A.R.
yihuizhang@tsinghua.edu.cn; jrogers@illinois.edu

doi:10.1038/natrevmats.2017.19
Published online 29 Mar 2017

The development of strategies for forming 3D micro- and nanostructures in advanced materials is of increasing interest, driven by the potential for creating material systems with fundamentally new characteristics and functionalities. The notion of engineered materials, sometimes referred to as metamaterials[1–5], has its most prominent origins in electromagnetic structures with properties that do not occur naturally, such as negative refractive index[4] and artificial magnetism[2]. Here, extended 3D arrays of interconnected features with dimensions in the subwavelength regime allow exquisite control over the propagation of electromagnetic waves, with impressive examples in the microwave[4,6–8], terahertz[9–11], and infrared and visible[12–16] regions of the electromagnetic spectrum. The required length scales span a wide range, from a few millimetres to tens of nanometres. The challenges in growth, assembly and/or fabrication are daunting, in which solutions require fundamental, conceptual advances in materials science and engineering. As examples, routes to 3D micro- and nanostructures for photonics include colloidal self-assembly[17], holographic lithography[18–21], direct-semiconductor or layer-by-layer growth[22–25], and two- or multiphoton lithography[26–29]. Fabrication typically begins with formation of the necessary 3D architectures in materials optimized for this purpose, followed by exchange and/or templated growth to convert these materials into those required to yield desired optical responses. For example, two- or multiphoton lithography provides a means for patterning 3D structures with geometries suitable for photonic bandgap behaviour, but only in specialized, photosensitive materials that do not possess a sufficiently high dielectric constant. Therefore, these 3D structures are often used as templates for forming thin films of metals or semiconductors by atomic layer or chemical vapour deposition[30–32].

Modern use of the term ‘metamaterial’ spans materials that have structurally engineered behaviours in any property of interest, including optical[12–16], thermal[33–35], acoustic[36–39], mechanical[40–48] and electromagnetic[4,6–8]. Progress in nearly all cases relies critically on developments in materials and methods for forming 3D

© 2017 Macmillan Publishers Limited, part of Springer Nature. All rights reserved.

Author addresses

[1]Center for Mechanics and Materials, AML, Department of Engineering Mechanics, Tsinghua University, Beijing 100084, China.
[2]Department of Materials Science and Engineering and Frederick Seitz Materials Research Laboratory, University of Illinois at Urbana-Champaign, Urbana, Illinois 61801, USA.
[3]Department of Electrical and Computer Engineering, University of Illinois at Urbana-Champaign, Urbana, Illinois 61801, USA.
[4]Departments of Civil and Environmental Engineering, Mechanical Engineering, and Materials Science and Engineering, Northwestern University, Evanston, Illinois 60208, USA.
[5]Departments of Materials Science and Engineering, Biomedical Engineering, Neurological Surgery, Chemistry, Mechanical Engineering, Electrical Engineering and Computer Science; Center for Bio-Integrated Electronics; and Simpson Querrey Institute for BioNanotechnology, Northwestern University, Evanston, Illinois 60208, USA.

structures. For example, recent work demonstrates mechanical metamaterials[40,42,43] in the form of ceramic and metallic micro- and nanolattices that reach previously inaccessible regimes of a parameter space defined by the strength, stiffness and weight. Advances in such types of mechanical metamaterials follow from the emergence of ingenious methods for multiphoton patterning and large-area projection micro-stereolithography (LAPμSL)[44] that provide access to hierarchical structures with disparate 3D features with length scales from nanometres to centimetres. Lightweight metamaterials with tunable 3D negative thermal expansion can be achieved with carefully designed 3D periodic lattice units containing constituents with varied thermal expansion coefficients[49]. This type of system can be realized with a multimaterial projection micro-stereolithography (PμSL) method in which two distinct beam constituents join to form composite microlattices[49]. Soft acoustic metamaterials can be formed with 3D structures that exhibit strong low-frequency Mie resonances[50–52]. In certain examples, microfluidic strategies yield macroporous silicone microbeads randomly dispersed in gel matrices, with negative acoustic phase velocity over a broad range of frequencies[50].

3D micro- and nanostructures also offer powerful engineering design options for microsystem technologies, with relevance to biomedical devices[53–57], microelectromechanical systems (MEMS)[58–60], energy storage platforms[61–66], optoelectronic components[67,68], and others[69] (for example, electronics[70–76]) where conventional, planar architectures currently dominate. As with metamaterials, progress follows from the ability to realize 3D structures in advanced materials. In addition to the optical techniques described previously, innovations in 3D printing techniques[77,78] and associated inks[70,79–86] based on metal, metal oxides, biomaterials and biocompatible polymers represent notable recent developments. Alternative methods that exploit concepts in origami, kirigami[87–92] and mechanically guided assembly[74,75,93–97] provide complementary capabilities, with key advantages that derive from compatibility with modern planar technologies and associated thin-film deposition and processing techniques.

This Review highlights the latest results and future trends in these types of techniques (that is, printing, folding, rolling and assembly) as routes to 3D mesostructures in advanced functional materials. The discussions begin with techniques for 3D printing that use scanning nozzles and patterns of light in schemes that utilize two-phonon lithography (TPL) and PμSL, including recent strategies that allow continuous, high-speed operation. Subsequent sections summarize methods based on folding and mechanical assembly, with application to materials such as designer hydrogels, monocrystalline inorganic semiconductors and graphene. We conclude by outlining some challenges and opportunities for future research.

Nozzle-based 3D printing technologies

The most widely used method for 3D printing relies on robotic control of scanning deposition nozzles in which 3D structures form in a layer-by-layer manner[85,98–101]. Materials typically formulated from particulate and/or polymeric species with desired rheological behaviour serve as 'inks'. Depending on the properties of the inks and the nature of the delivery process, these techniques can be further classified into two groups[85,98,102]: inkjet printing for liquid inks and microextrusion printing for viscoelastic inks (FIG. 1a).

Inkjet printing, also known as drop-on-demand printing, exploits nozzles that use thermal or acoustic processes to deliver liquid droplets to desired locations on the substrate[85,98,102–104]. By contrast, microextrusion printing uses pressure-induced flow to form continuous filaments of material, often designed to solidify immediately or shortly after emergence from the nozzle tip. In both cases, proper materials formulation is essential. For inkjet printing, the challenges are in realizing high solid content for thick deposits, but at sufficiently low viscosity to allow droplet generation in a manner that also avoids clogging of the nozzles[105]. Although inkjet printing has widespread applications in forming 2D structures, 3D architectures can be difficult to form, partly owing to the uncontrolled flow of inks as they impinge on a structured surface[106].

By comparison, microextrusion printing offers far greater possibilities in 3D structuring owing to the broad range of ink designs and feature sizes. Microextrusion printers that offer modest (slightly sub-millimetre) resolution are now widely available in the form of commercial, user-friendly tools. In most cases, a printing head robotically controls the extrusion of a material ink onto a substrate, whereby a handling and dispensing system pneumatically or mechanically (with a piston or screw) controls the extrusion of materials in well-defined ambient conditions[85].

Recent research establishes methods for fabricating sophisticated 3D mesostructures with microscale resolution in a broad range of materials, including concentrated colloidal[107], nanoparticle[108], fugitive[83,109] and polyelectrolyte[110] inks. Main areas of current interest are in conductive and biomaterial inks because of their relevance in key applications, from solid-state lighting and wearable devices to tissue scaffolds and regenerative medicine. The following subsections highlight some of the latest progress.

© 2017 Macmillan Publishers Limited, part of Springer Nature. All rights reserved.

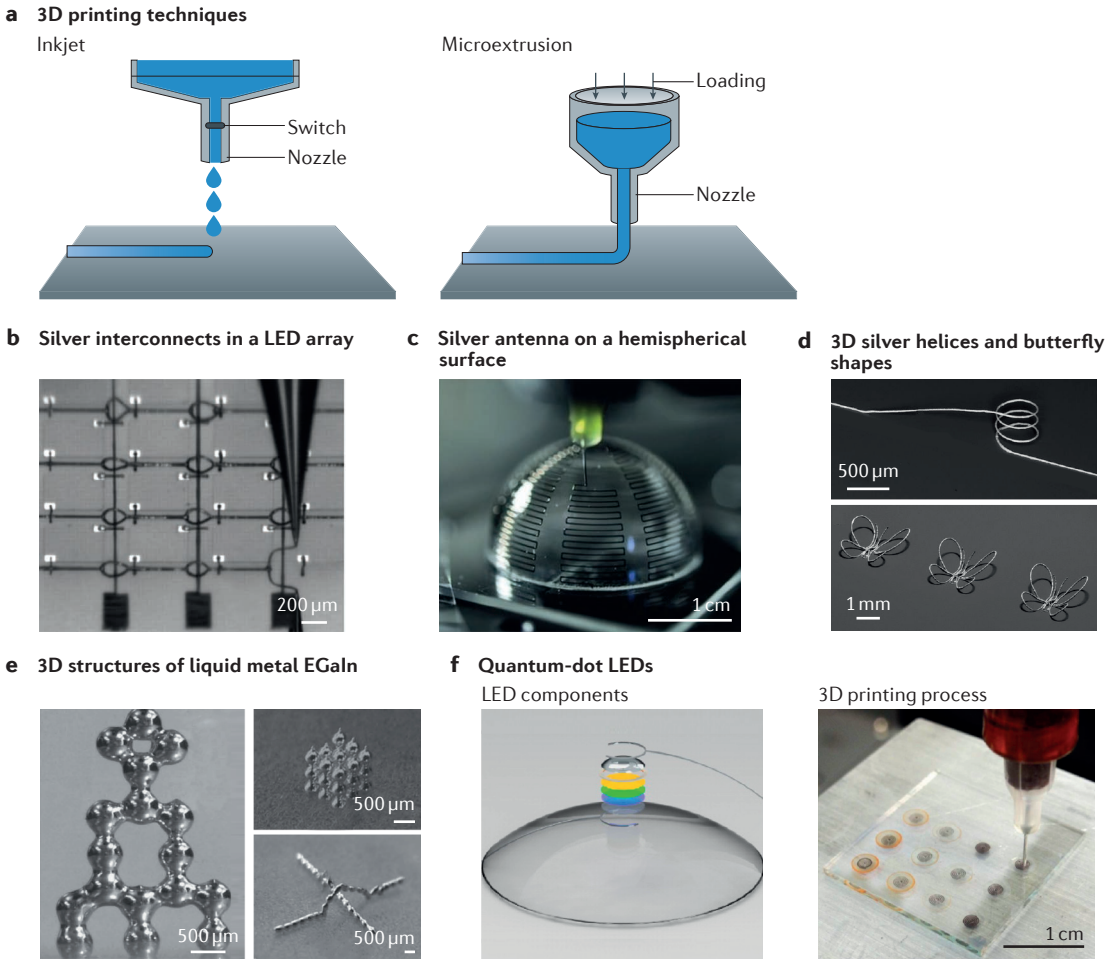

Figure 1 | **Nozzle-based 3D printing technologies and applications in conductive structures. a** | Schematic illustration of nozzle-based inkjet (left) and microextrusion (right) printing techniques. Inkjet printing usually relies on thermal or acoustic processes to deliver liquid droplets to desired locations on a substrate. Microextrusion printing uses pressure-induced flows to form continuous filaments of material, often designed to solidify immediately or shortly after emergence from the nozzle tip. **b** | 3D silver interconnects between an array of microscale light-emitting diodes (LEDs). **c** | A 3D silver antenna printed onto a hemispherical surface. **d** | 3D silver helices and butterfly shapes. **e** | 3D structures printed with the liquid metal EGaIn. **f** | Schematic illustration of quantum-dot LED components and an optical image acquired during 3D printing of this multimaterial structure. Panel **b** is adapted with permission from REF. 70, AAAS. Panel **c** is adapted with permission from REF. 79, Wiley-VCH. Panel **d** is adapted with permission from REF. 80, National Academy of Sciences. Panel **e** is adapted with permission from REF. 82, Wiley-VCH. Panel **f** is adapted with permission from REF. 84, American Chemical Society.

3D printing with conductive inks. One notable advance[70,79,80] involves highly concentrated silver nanoparticle inks (>70 wt% Ag) for electrically conductive filaments in 3D arrangements (FIG. 1b,c). The viscoelastic properties enable self-supporting structures, such as the arc-shaped features in FIG. 1b. Thermal annealing (for example, at 150–500 °C) performed after printing by convective heating[70] or during printing by heating with a focused laser beam[80] can substantially improve the conductivity and the mechanical properties[70]. As shown in FIG. 1d, 3D helical coils and butterfly shapes can be formed by heating during printing[80]. Electrically functional devices, such as 3D spanning interconnects in arrays of microscale light-emitting diodes (FIG. 1b) and hemispherical antennas (FIG. 1c), suggest broad utility in electronics and optoelectronics[70,79].

Other strategies use liquid-metal inks in the form of binary eutectic alloys of gallium and indium (EGaIn)[81–83]. EGaIn is a low-viscosity liquid at room temperature (with a melting point of ~15.7 °C). An ultrathin (~1 nm) passivating layer of gallium oxide forms immediately on exposure to air, thereby preventing spontaneous flow in ambient conditions[81]. As a result, at modest pressures (<5 kPa), metal filaments of EGaIn can be extruded to form free-standing structures. Additional options include the formation of 3D architectures of stacked droplets (FIG. 1e) delivered with a nozzle or of bars formed by the injection of metal into 3D microchannels created in sacrificial materials[82,83].

Sophisticated function in 3D structures typically demands the integration of several different types of materials, including, but not limited to, metals.

© 2017 Macmillan Publishers Limited, part of Springer Nature. All rights reserved.

Achieving compatibility between different printed materials represents an additional challenge. In one successful example, a sequential printing process forms quantum-dot light-emitting diodes[84] (FIG. 1f) that incorporate five different materials, including emissive semiconductor nanoparticles, conductive polymers, solid or liquid metal leads, a transparent substrate and an elastomeric matrix, all in a 3D architecture. Another notable achievement is in multimaterial 3D printing of rechargeable lithium-ion microbatteries with high areal energy and power densities[66].

Despite these advances, existing methods in 3D printing cannot readily produce customized, fully integrated 3D electronic devices in a scalable manner. Opportunities exist in the development of advanced functional inks and flexible printing platforms (for example, multi-nozzle print heads) for rapid and precise patterning of materials over a broad range of compositions and ink-flow behaviours[105].

3D printing of biomaterials. Methods for 3D printing that are similar to those described above allow precise layer-by-layer positioning of biomaterials, living cells and/or biocompatible polymers into 3D structures with relevance to biology research and clinical medicine. As with applications in semiconductor devices, this type of bioprinting involves a complex interplay between geometry and material types, with the additional distinction that the resulting systems must accommodate time-dependent interactions with living systems, in which cell types, growth factors and dynamical mechanical and chemical effects can be critical[85]. Nevertheless, recent advances enable the reproduction of certain key features of the complex microstructure of the extracellular matrix, including compatibility with multiple cell types and at sufficient resolution and fidelity to recapitulate biological function[85]. For example, nozzles with diameters of 100–400 μm and inks of gelatin and fibrinogen that contain multiple cells and fugitive material of Pluronic F127 can be used to form thick (>1 cm and >10 cm^3 in volume) artificial tissues with embedded vessels (<1 mm in diameter)[111]. In a series of studies on synthetic heart valve conduits[112–114], biocompatible hybrid hydrogel inks patterned by 3D printing[115] yielded tissue constructs with thicknesses of ~1 mm and diameters of ~2 cm. In other examples[116], cartilage bodies with diameters and heights of 4 and 2 mm, respectively, result from inkjet printing with inks of poly(ethylene glycol) dimethacrylate and human chondrocytes, at layer thicknesses of 18 μm. Details of these efforts appear in other reviews[85,102]. The main technological challenges are in increasing the resolution and manufacturing speed for clinically relevant sizes with a broadened set of biocompatible materials and an ability to maintain cellular viability and function. Additional opportunities exist in the heterogeneous integration of multiple biomaterials or of biomaterials with spatial gradients of compositions to achieve desired functional and mechanical properties. Printing of adaptive biomaterials with shapes, properties or functions that can be reprogrammed on demand represents an additional intriguing direction[85].

Two main areas of application are in synthetic tissues and organs for tissue engineering and for regeneration, with representative examples summarized in FIG. 2. An impressive range of synthetic tissues and organs can now be realized, including heart valve conduits[112–114], ear-shaped bionic structures[117], tissue-engineered bones[118–120], vascular networks[111,121] and certain components of the nervous system[122]. Bone scaffolds can be engineered with cellular microstructures that provide superior hyperelastic properties, including the ability to enable osteogenic differentiation of stem cells *in vivo* with or without osteo-inducing factors[118–120]. Moreover, thick, heterogeneous cell-laden tissues can be perfused with printed vascular networks in a way that differentiates human mesenchymal stem cells towards an osteogenic lineage *in situ*[111,121]. Another class of application relates to tissue regeneration and repair. Recent advances in skin and nerve regeneration[123,124] and cartilage repair[116,125] suggest great potential in these areas. For example, artificial, printed skin-like structures can be used for applications in wound closure, re-epithelialization and neovascularization of regenerating skin[123]. Printed nerve scaffolds can be used in nerve regeneration following complex injuries, with the final pathway geometry adapted to the original tissue structure, in which physical and biochemical cues provide axonal guidance for bifurcating pathways[124].

Light-based 3D writing technologies

3D writing techniques that rely on patterned exposure of materials to light usually involve locally induced two- or multiphoton polymerization[26,27,126–128], UV photocuring[129–131] or selective melting[132]. In contrast to nozzle-based methods, these techniques only operate effectively with a narrow range of materials, but they offer exceptionally high resolution and speeds of printing. This section focuses on three of the most promising techniques: TPL[26,27,126–128], PμSL[43,44,131,133] and continuous liquid interface production[77,78,134], with highlights in applications for ultralight and ultrastiff mechanical metamaterials.

Two-photon lithography. In this approach, specially formulated photopolymers absorb two photons, typically in the infrared region of the spectrum, in a single quantum event, the collective energy of which corresponds to blue or near-UV light. As the rate of two-photon absorption is proportional to the square of the light intensity, absorption occurs preferentially at the waist of a highly focused laser beam, thereby confining the polymerization process to a volumetric region with sub-micrometre dimensions, often beyond the diffraction limit[135]. A typical fabrication system consists of a collection of focusing lenses and beam-steering optics, a laser and a 3D scanning stage that supports a liquid bath of the photopolymer (FIG. 3a, left). As the focused laser beam scans laterally in the photopolymer and the stage scans vertically, the point of focus moves in a 3D trajectory under computer control, thereby enabling the fabrication of a desired 3D microstructure with ultrahigh resolution. Many schemes exist to improve the resolution (for example, to the sub-30 nm regime) and to expand the applicable material types, as summarized in other review articles[29,135].

© 2017 Macmillan Publishers Limited, part of Springer Nature. All rights reserved.

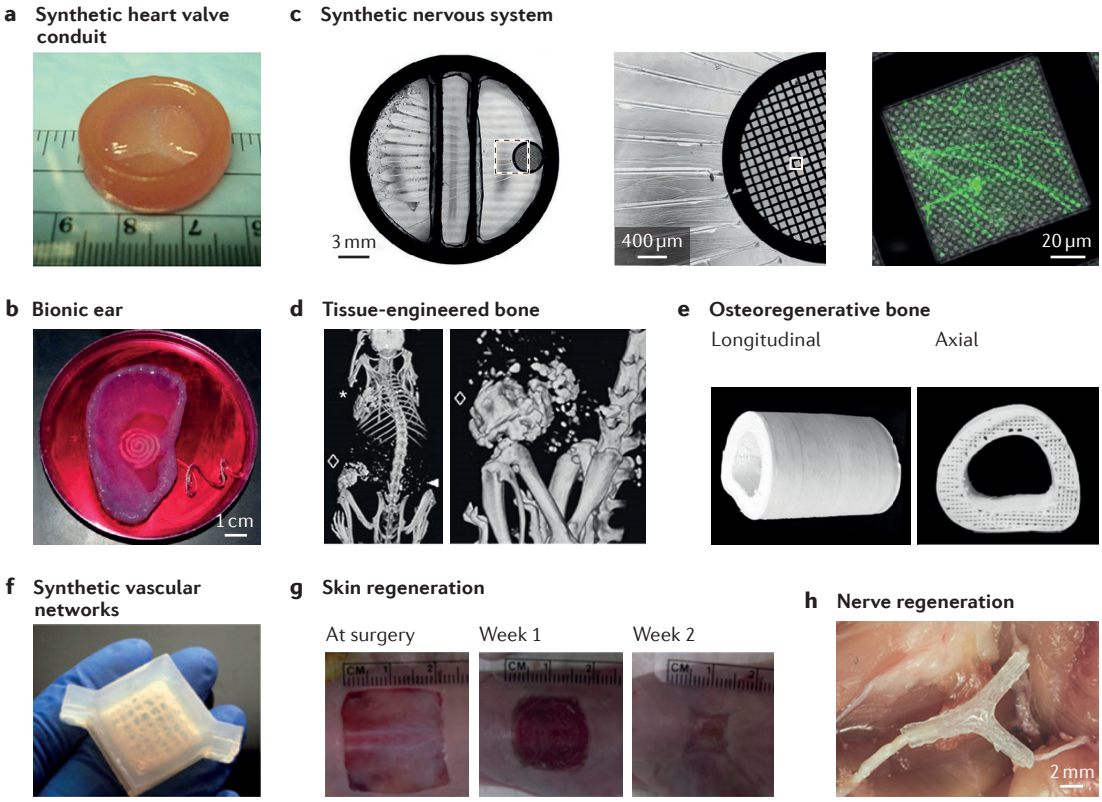

Figure 2 | **Applications of nozzle-based 3D printing technologies in 3D bioprinting. a** | Synthetic heart valve conduit. **b** | Bionic ear. **c** | Synthetic nervous system. **d** | Tissue-engineered bone. **e** | Osteoregenerative bone. **f** | Synthetic vascular networks. **g** | Skin regeneration. **h** | Nerve regeneration. Panel **a** is adapted with permission from REF. 113, Elsevier. Panel **b** is adapted with permission from REF. 117, American Chemical Society. Panel **c** is adapted with permission from REF. 122, Royal Society of Chemistry. Panel **d** is adapted with permission from REF. 118, Macmillan Publishers Limited. Panel **e** is adapted with permission from REF. 119, AAAS. Panel **f** is adapted with permission from REF. 111, National Academy of Sciences. Panel **g** is adapted with permission from REF. 123, AlphaMed Press. Panel **h** is adapted with permission from REF. 124, Wiley-VCH.

Owing partly to the remarkable spatial resolution that can be achieved, many advanced applications are possible in photonic metamaterials[16,30–32,136–138], MEMS and nanoelectromechanical systems (NEMS)[139–142], electronics[143–146] and mechanical metamaterials[41,42,147,148]. Mechanical metamaterials are of particular interest in the context of TPL because their mechanical properties can be defined not only by the geometries of the 3D architectures, but also by the ability to reduce the characteristic length scales (that is, several or tens of nanometres) to regimes in which size effects in material properties are pronounced.

To bypass materials constraints set by requirements for two-photon sensitivity, the 3D structures formed by TPL can serve as sacrificial templates for atomic-layer deposition, sputtering or plating of metals or ceramics to form nanolattices of these materials[41,42,147–150]. The resulting systems have feature sizes that can extend to the nanoscale with, for example, wall widths and thickness in the ranges of 150–500 nm and 5–600 nm, respectively[41,42,147,148,151,152]. Nanolattices of alumina are shown in FIG. 3a (middle), in which the hollow cross-sections of the constituent beams provide ultralight-weight construction[42]. Mechanical testing indicates that ceramic metamaterials of this type combine parameters of weight and strength (FIG. 3a, right) that are beyond those possible with the corresponding materials in unpatterned form. For example, such nanolattices have an ability to recover their original shape after compressive strains of 50% or more, owing to stretching-dominated deformations and elastic shell buckling in 3D architectures engineered for this purpose. Hierarchical metamaterials with fractal-inspired lattice layouts are also possible, as shown by recent studies of polymer, hollow ceramic and polymer–ceramic composites[147]. Further developments are necessary, however, to increase the patterning speeds and scalability (that is, manufacturing a large number of small-scale components in a reasonable time) needed for practical applications.

Projection micro-stereolithography. As in traditional stereolithography, PμSL forms complex 3D mesostructures in a layer-by-layer manner based on photopolymerization reactions in resin materials[43,131,133]. Each layer corresponds to a 2D image of a sectional slice of a desired 3D shape, formed by projection through a spatial light modulator using a demagnifying lens system. Exposure to UV light solidifies the liquid resin to

© 2017 Macmillan Publishers Limited, part of Springer Nature. All rights reserved.

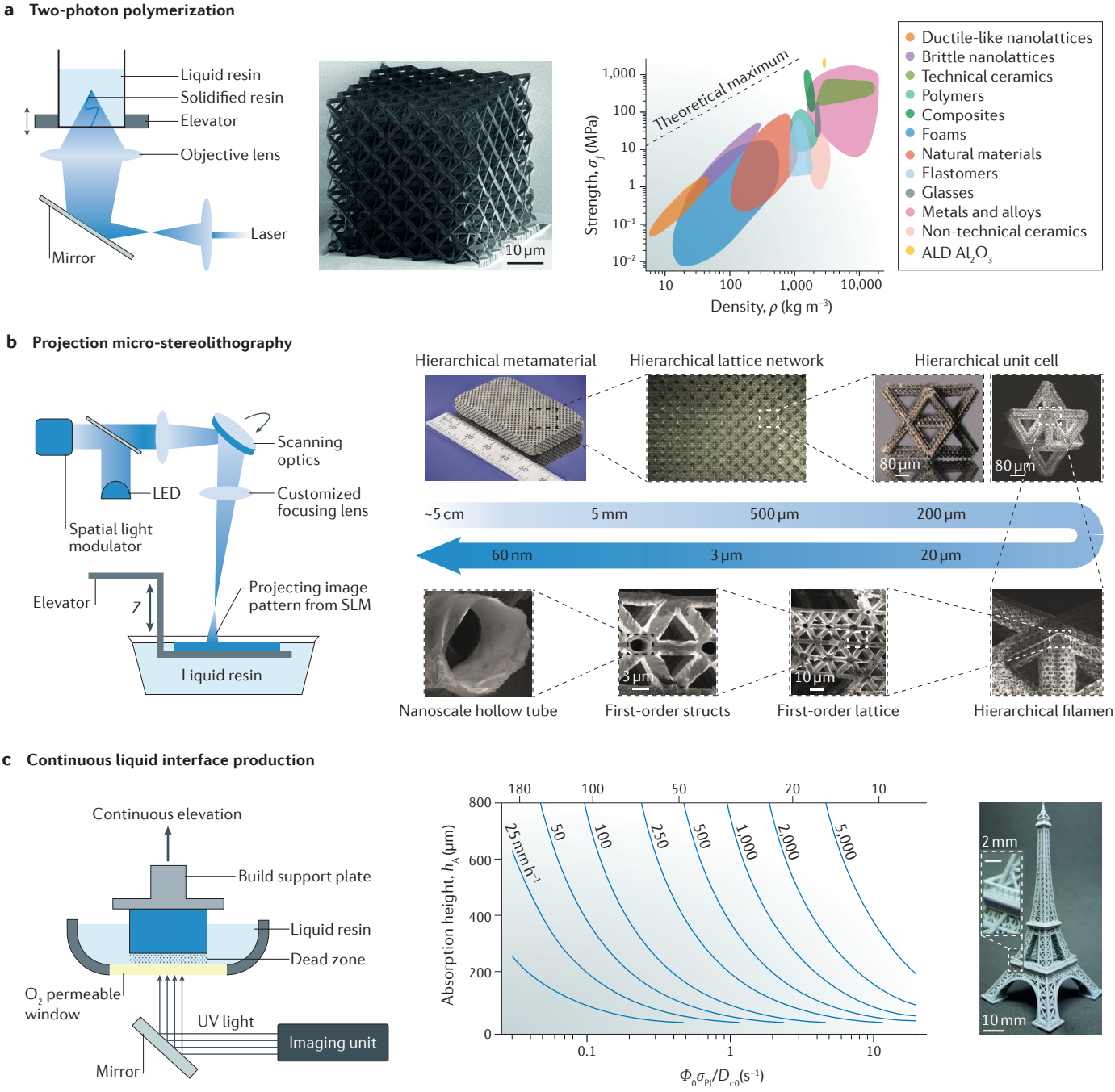

Figure 3 | **Light-based 3D printing technologies: schemes, structures and properties. a** | Multiphoton polymerization: schematic illustration in which a highly focused laser beam polymerizes photopolymers by two-photon effects in volumetric regions with sub-micrometre dimensions (left). Scanning electron micrographs of an alumina octet-truss nanolattice (middle). Strength as a function of density for various materials (right). **b** | Large-area projection micro-stereolithography (LAPμSL): schematic illustration in which a portion of a 2D image (corresponding to a sectional slice of a desired 3D shape) is formed by projection through a spatial light modulator (SLM), and then directed dynamically through an optical scanning system onto a corresponding region of the resin to solidify the entire 2D layer of the liquid resin (left). Optical microscope images and scanning electron micrographs of a hierarchical 3D metamaterial fabricated by LAPμSL, with a cross-sectional highlight of its structural hierarchy (right). **c** | Continuous liquid interface production (CLIP): schematic illustration in which an oxygen-permeable window creates a narrow, oxygen-inhibited zone to locally prevent photopolymerization, thereby allowing for simultaneous UV exposure, resin renewal and elevation of the build support plate (left). CLIP print speed as a function of the characteristic optical absorption height and the combined parameter $\Phi_0\alpha_{PI}/D_{c0}$ (middle). Eiffel Tower model printed using CLIP (right). Panel **a** (middle and right) is adapted with permission from REF. 42, AAAS. Panel **b** is adapted with permission from REF. 44, Macmillan Publishers Limited. Panel **c** is adapted with permission from REF. 78, AAAS.

© 2017 Macmillan Publishers Limited, part of Springer Nature. All rights reserved.

form a thin, solid 2D layer in the geometry of the image. Lowering the substrate, coating the pattern with uncured resin and then repeating the process eventually completes the 3D fabrication. This scheme provides excellent structural diversity, with resolution in the micrometre range over areas of several centimetres[43], comparable to that achieved with a photopolymer waveguide technique[40]. The parallel operation enables speeds that are much higher than those of serial approaches such as TPL and nozzle-based printing. However, traditional methods have limited fields of view and associated difficulties in forming hierarchical geometries with diverse feature sizes over large areas.

A recent variant — large-area projection micro-stereolithography (LAPμSL)[44] — overcomes these disadvantages through the use of an optical scanning system that dynamically directs a portion of the 2D image onto a corresponding region of the resin in a coordinated, sequential manner to complete the entire 2D layer (FIG. 3b, left). The power of LAPμSL is demonstrated by the formation of metallic hierarchical lattices with different structural topologies, for which the minimum feature size (50 nm) is several orders of magnitude smaller than the overall size of the sample (~5 cm)[44] (FIG. 3b, right). An alternative approach combines PμSL with methods based on folding or mechanically guided assembly in an integrated approach to allow for rapid formation of hierarchical lattices or other 3D architectures with diverse feature sizes.

Continuous liquid interface production. Dramatic improvements in micro-stereolithography follow from ideas that eliminate the need to coat the resin after each exposure. The key concept involves an oxygen-permeable window that creates a narrow, oxygen-inhibited zone to locally prevent photopolymerization, and an exposure system that illuminates the resin bath through this window from beneath[77,78] (FIG. 3c, left). Specifically, this setup incorporates a thin, uncured liquid layer (that is, a dead zone) between the window and the photopolymerized resin, where oxygen quenches the photoexcited photoinitiator. This lubricating film allows for simultaneous UV exposure, resin renewal and platform (that is, a build support plate) movement in the upward direction, thereby avoiding the separate, discrete steps required in traditional micro-stereolithography. The resulting process, known as continuous liquid interface production, offers throughputs that are much higher than those previously possible, typically by more than an order of magnitude[77,78]. The thickness of the dead zone depends on the incident photon flux (Φ_0), the photoinitiator absorption coefficient (α_{PI}) and the curing dosage (D_{c0}), according to $(\Phi_0\alpha_{PI}/D_{c0})^{-0.5}$ (REF. 78). As a consequence, the print speed approximately scales with the combined parameter $(\Phi_0\alpha_{PI}/D_{c0})$ and the absorption height (that is, the resolution) of the resin for geometries in which the speed-limiting process is resin curing (FIG. 3c, middle). For target geometries with comparatively wide solid cross-sections, these predictions of print speed do not apply, because the flow of resin into the building area becomes a dominant consideration. Complex 3D mesostructures, for example, the Eiffel Tower in FIG. 3c (right), can be drawn out of a resin bath at rates of hundreds of millimetres per hour. This rate of production has some potential for use in high-volume manufacturing of delicate microscale parts, such as microneedles for transcutaneous drug delivery[134].

Stress-controlled folding of 3D systems

A set of strategies that complement the direct fabrication routes described previously exploits stress-controlled folding and/or mechanically guided assembly of 2D precursor structures. Such schemes fully leverage the sophisticated technologies that exist for micro- and nanofabrication, and for materials deposition in the semiconductor and integrated photonic industries, ranging from patterning methods (for example, projection-mode photolithography) to processing techniques (for example, etching and thin-film deposition) and material growth strategies (for example, epitaxial growth and doping). This section focuses on methods for folding induced by internal stresses, including two classes of advanced techniques based on 4D printing and micro- and nanoscale origami. A subsequent section reviews strategies of mechanically guided, deterministic assembly via forces imposed by a supporting substrate.

4D printing. In this scheme, 3D printing techniques form structures that have a bilayer or multilayer heterogeneous design with mismatched strains that follow from external stimulation — for example, exposure to water or heat — thereby inducing self-folding or self-rolling into 3D shapes that are responsive to their environment and/or would be difficult to print directly. Representative material systems include hydrogels[153–155] and shape-memory polymers (SMPs)[156–158].

One example of hydrogel-based 4D printing uses a composite ink in programmable bilayer architectures[153], wherein the constituent filaments exhibit anisotropic stiffness and swelling behaviour (FIG. 4a). Differential swelling between the top layer and bottom layer leads to controlled folding deformations and spatially varying curvatures that depend mainly on the elastic moduli, the swelling ratios, the thickness ratio of two different layers and the total bilayer thickness. Quantitative mechanics models that extend the classical Timoshenko theory for bimetallic strips can capture all of these effects, allowing predictions of the final, fully hydrated state. Reversible changes in 3D configuration are possible with stimuli-responsive (for example, temperature) hydrogels[153]. The hydrogel can also be laminated against a passive polymeric material to form a self-evolving joint capable of folding, curling, twisting, and linear expansion or shrinkage, on exposure to water[154,155].

In SMP-based 4D printing[156], 3D-printed bilayer structures comprise a matrix and a laminate with embedded SMP fibres (FIG. 4a). Controlled 3D transformation can be achieved by stretching at temperatures above the characteristic transition of the SMP, followed by cooling and releasing the externally applied force. Impressive examples of dynamically changing 3D structures can be achieved with different material systems (FIG. 4b), such as

© 2017 Macmillan Publishers Limited, part of Springer Nature. All rights reserved.

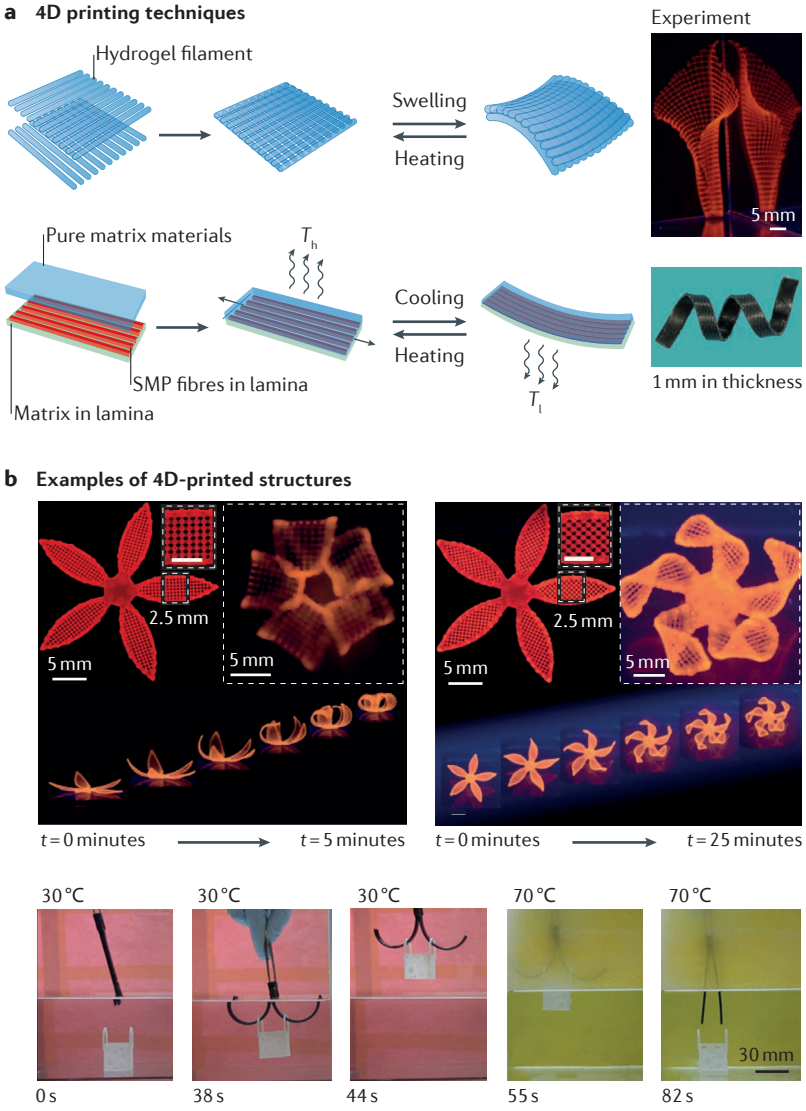

Figure 4 | **4D printing schemes and time-evolving structure geometries. a** | Schematic illustration of two 4D printing techniques and images of representative structures. The schematic illustration on the top shows a 3D-printed hydrogel bilayer composite, in which differential swelling between the top layer and bottom layer induces controlled folding deformations, leading to time-evolving 3D transformation from the original 2D shape. The schematic illustration on the bottom shows a 3D-printed bilayer structure of a matrix and a laminate with embedded shape-memory polymer (SMP) fibres, which can achieve controlled 3D transformation through the action of strain in the SMP developed by changes in temperature across the glass transition point (T_g). **b** | Two hydrogel patterns with flower geometries and different petal patterns, with time-lapse images that illustrate the geometrical transformation induced by swelling (top). Application of SMP-based 4D printing to form a programmable hook, in which a small box is lifted up from a container immersed in water at 30 °C, and then released into another water-filled container at 70 °C (bottom). T_h, a temperature higher than T_g; T_l, a temperature lower than T_g. Panel **a** is adapted with permission from REF. 153, Macmillan Publishers Limited, and REF. 156, AIP Publishing. Panel **b** (top) is adapted with permission from REF. 153, Macmillan Publishers Limited. Panel **b** (bottom) is adapted with permission from REF. 158, Macmillan Publishers Limited.

a programmable hook that can grasp objects and then release them using a thermal switching mechanism. An intriguing future direction is in the development of new printable materials that can respond to external stimuli at desired rates.

Micro- and nanoscale origami. Folding deformations can serve as the basis for origami-inspired assembly at micro- or nanoscales[69,159–162]. In most published examples, the necessary forces arise from capillarity, thin-film residual stresses or mechanically active (that is, stimuli responsive) materials. As an example of capillary forces[163–168], heating a solder above its melting point drives the folding of adjacent panels as the solder reconfigures its shape to minimize the surface energy (FIG. 5a, left). Water droplets can also provide sufficient capillary forces for this type of origami assembly[89,90]. Various classes of closed-form polyhedral mesostructures can be realized in this manner[89,167,168], with representative examples in FIG. 5b.

Schemes based on thin-film residual stresses typically rely on strain mismatch between different materials in a multilayer stack to induce self-rolling upon removal of an underlying sacrificial layer[169–172]. A schematic illustration of this strategy is shown in FIG. 5a (middle), in which a strain gradient along the thickness direction can be controlled through relevant parameters (for example, temperature, frequency, composition and deposition rates) associated with the thin-film deposition process. This strategy can produce mesostructures with tubular, scroll-like or polyhedral geometries, in a range of material systems (for example, Pt, ZnO, Al_2O_3, Si_xN_y, TiO_2, SiGe, Si_xN_y–Ag, InGaAs–GaAs and Pd–Fe–Pd)[71–73,91,169,170,173–180]. Examples of tubes achieved in this way are shown in FIG. 5c.

Another strategy involves active materials (for example, hydrogels[181–186], SMPs or shape-memory alloys (SMAs)[187–189], liquid crystal elastomers[190,191] or photoactive polymers[192,193]) to create spatially non-uniform strains, either along the in-plane or out-of-plane (that is, thickness) directions, thereby deforming planar structures into desired 3D shapes. A schematic illustration appears in FIG. 5a (right), in which a multilayer hydrogel design provides a folding mechanism similar to that based on thin-film residual stresses. This scheme offers a high degree of flexibility in hierarchical 3D design (FIG. 5d). In the examples of FIG. 5b–d, the final 3D configuration typically represents a state of equilibrium that results from minimization of the total system energy, which consists of the strain energy (in terms of bending energy and membrane energy for various layers within the thin films) and the work done by an external force (for example, capillary forces). This total energy can be expressed as functions of local curvatures according to mechanics models, which then define relationships between the various driving forces, the geometric parameters and the curvature of the target surfaces.

Compatibility of strategies based on capillary forces and thin-film residual stresses with established planar technologies suggests potential for building new classes of 3D electronic, optoelectronic and biomedical devices. Examples include solar cells with improved efficiency in light harvesting[90], cell grippers capable of separating and isolating single cells[178], antennas that allow implantation using standard medical syringes[175], and inductors for radio-frequency-integrated circuits with extremely small form factors and improved electrical performance, particularly at frequencies for 5G wireless communication

© 2017 Macmillan Publishers Limited, part of Springer Nature. All rights reserved.

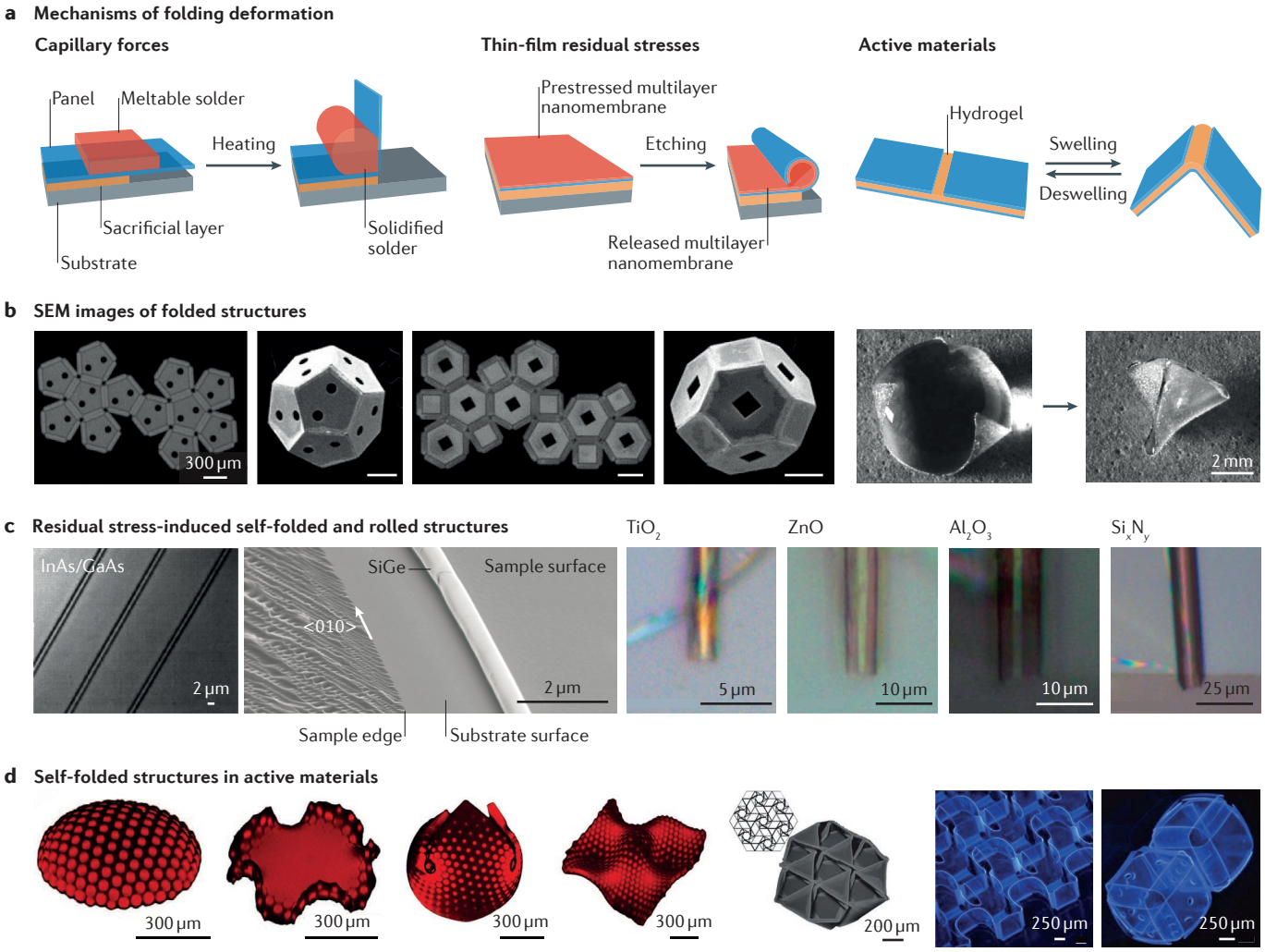

Figure 5 | **Micro- and nanoscale origami: schemes, structures and device applications. a** | Schematic illustrations of methods that rely on capillary forces (left), thin-film residual stress (middle) and active materials (right). **b** | Optical and scanning electron microscope (SEM) images of folded structures formed using capillary forces, including a dodecahedron and an octahedron of nickel, and a tetrahedron of polydimethylsiloxane. **c** | Optical and SEM images of residual-stress induced self-folded or rolled structures in a range of materials. **d** | Self-folded structures in active materials: hydrogels (left five images) and photopatterned polymers (right two images). Panel **b** (four images, left) is adapted with permission from REF. 168, National Academy of Sciences. Panel **b** (two images, right) is adapted with permission from REF. 89, American Physical Society. Panel **c** is adapted with permission from REF. 169, Elsevier; REF. 170, Macmillan Publishers Limited; and REF. 176, Wiley-VCH. Panel **d** is adapted with permission from REF. 182, AAAS; REF. 183, Wiley-VCH; and REF. 192, Macmillan Publishers Limited.

and beyond[76,194]. Remaining challenges are in achieving reversible and programmable self-folding of high-performance materials at micro- or nanoscale. Opportunities exist in the development of techniques for the micro- and nanoscale patterning of 2D thin films of active materials (for example, SMP or SMA) and their heterogeneous integration with passive layers of high-performance, electronic materials.

Recent studies explore the fundamental limits of this type of process, using graphene as either the structural material or the material at the primary locations of bending[92,195]. The atomic-scale thickness of graphene leads to the possibility for exceptionally small radii of curvature. Graphene with kirigami-inspired patterns and lateral feature sizes of ~2 μm can be assembled into 3D configurations under in-plane or out-of-plane loading[92] (FIG. 6a,b). In these examples, mechanical stages, magnetic forces or other externally imposed stimuli drive the assembly. Self-tearing or peeling of graphene from a substrate by thermal activation can also lead to folding deformations[195], thereby providing a route to origami processes (FIG. 6c). Atomistic simulations provide insights into the underlying physics[196–201].

Mechanically guided assembly

The techniques described above apply most readily to plates or simple curved structures (for example, tubes and scrolls), where the most sophisticated 3D geometries consist of closed- or open-form polyhedra and their variants, or cylindrical structures. Recently introduced approaches

© 2017 Macmillan Publishers Limited, part of Springer Nature. All rights reserved.

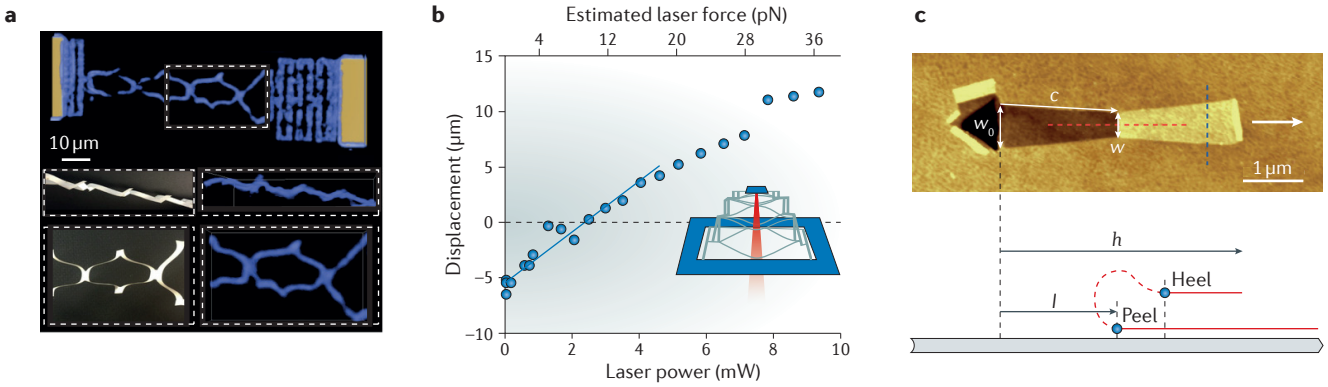

Figure 6 | **Graphene origami and kirigami. a** | 3D reconstruction from a *z*-scan focal series of images of a spring made from graphene with a lithographically defined pattern of cuts, with insets that show side and top views of sections of the graphene (right) and corresponding paper models (left). **b** | Measurements of displacement as a function of laser force for a graphene pyramid, with a schematic shown in the inset. **c** | Atomic force microscopy image of a folded graphene ribbon and schematic illustration of a side view of the ribbon, featuring the fold cross-section with excess length $\zeta = 2l - h$ (dashed red curve between surface peel and heel points, indicated by blue dots). *c*, path length of the two tears (assumed to be identical) that define the ribbon shape; w_0, nucleation fold width; *w*, final fold width. Panels **a** and **b** are adapted with permission from REF. 92, Macmillan Publishers Limited. Panel **c** is adapted with permission from REF. 195, Macmillan Publishers Limited.

based on mechanically guided assembly involve precisely controlled, deterministic 2D–3D transformations[74] that expand the range of accessible 3D geometries, while maintaining compatibility not only with the methods described in the previous sections, but also with 2D microsystems technologies.

This process begins with the formation of a thin 2D precursor on a source wafer or other planar substrate, followed by the release and then precise patterning of regions that establish strong sites of adhesion to a pre-stretched elastomeric substrate (that is, an assembly platform) upon contact[74,75,93,95] (FIG. 7a). Release of the prestretch induces compressive forces at the bonding sites. The result causes the 2D precursor to geometrically transform, through spatially dependent deformations and in- and out-of-plane translational and rotational motions, into an engineered 3D configuration. The effect provides access to wide-ranging classes of topologies, for which the key control variables include: the 2D layout, thicknesses and mechanical properties of the precursor structures; the pattern of sites for selective bonding; and the nature and magnitude of the prestrain in the assembly platform.

Quantitative mechanics modelling can capture all of these factors at a precise quantitative level across 3D configurations with a rich diversity of complex shapes[74,75,93–95]. As an example, an elaborate 3D mesostructure formed of ribbons of device-grade, monocrystalline silicon is shown in FIG. 7b. The layout consists of a concentric pair of toroids and a separate hemispherical 'cage' construct at the centre. Guided by mechanics modelling, a wide range of filamentary mesostructures are possible[74], from helices, toroids and conical spirals, to structures that resemble spherical baskets, cuboid cages, starbursts, flowers, scaffolds and frameworks, each with single- and/or multiple-level configurations (FIG. 7c).

A broadened range of options follows from kirigami- or origami-inspired designs in the precursors[93,95,96]. For example, engineered variations of thickness in the 2D precursors can guide folding deformations at specific, targeted locations, owing to the cubic dependence of the bending stiffness on thickness. 3D mesostructures composed of membranes, plates, ribbons and wires, with continuously curved shapes and/or sharp folds between flat constitutive elements, can be achieved (FIG. 7d,e). The use of releasable, multilayer 2D precursors allows dense 3D architectures (FIG. 7f) with nested layouts, controlled points of entanglement and other features that are unobtainable with single-layer 2D precursors[75]. In addition, the elastomeric substrate itself can be engineered to achieve non-uniform distributions of strain in the pre-stretched state. The result provides desired strain fields for complex but well-defined control over the resultant 3D geometries[97].

An appealing feature of this scheme is that it has immediate, broad applicability to nearly any type of material, including inorganic semiconductors, metals, polymers and various heterogeneous combinations, spanning length scales from sub-micrometre to metre dimensions. FIGURE 8a highlights two 3D structures with length scales that range from sub-micrometre, to micrometre, millimetre, centimetre and metre dimensions[202]. The use of a diverse collection of materials (for example, Ni, Au, epoxy (SU8), polyimide, SU8–Au and SU8–Si) is also possible (FIG. 8b). Compatibility with state-of-the-art 2D fabrication, processing and growth techniques allows the transformation of virtually any type of existing 2D microsystem technology into a 3D configuration, thereby providing unusual design options and unique devices. Examples range from mechanically tunable spiral micro-inductors[74], the quality factor and resonance frequency of which can be adjusted in a reversible manner through deformations of the elastomer substrate (FIG. 8c), to near-field communication devices[75] that offer improved enhanced quality factor and expanded working angles compared with those of conventional 2D

© 2017 Macmillan Publishers Limited, part of Springer Nature. All rights reserved.

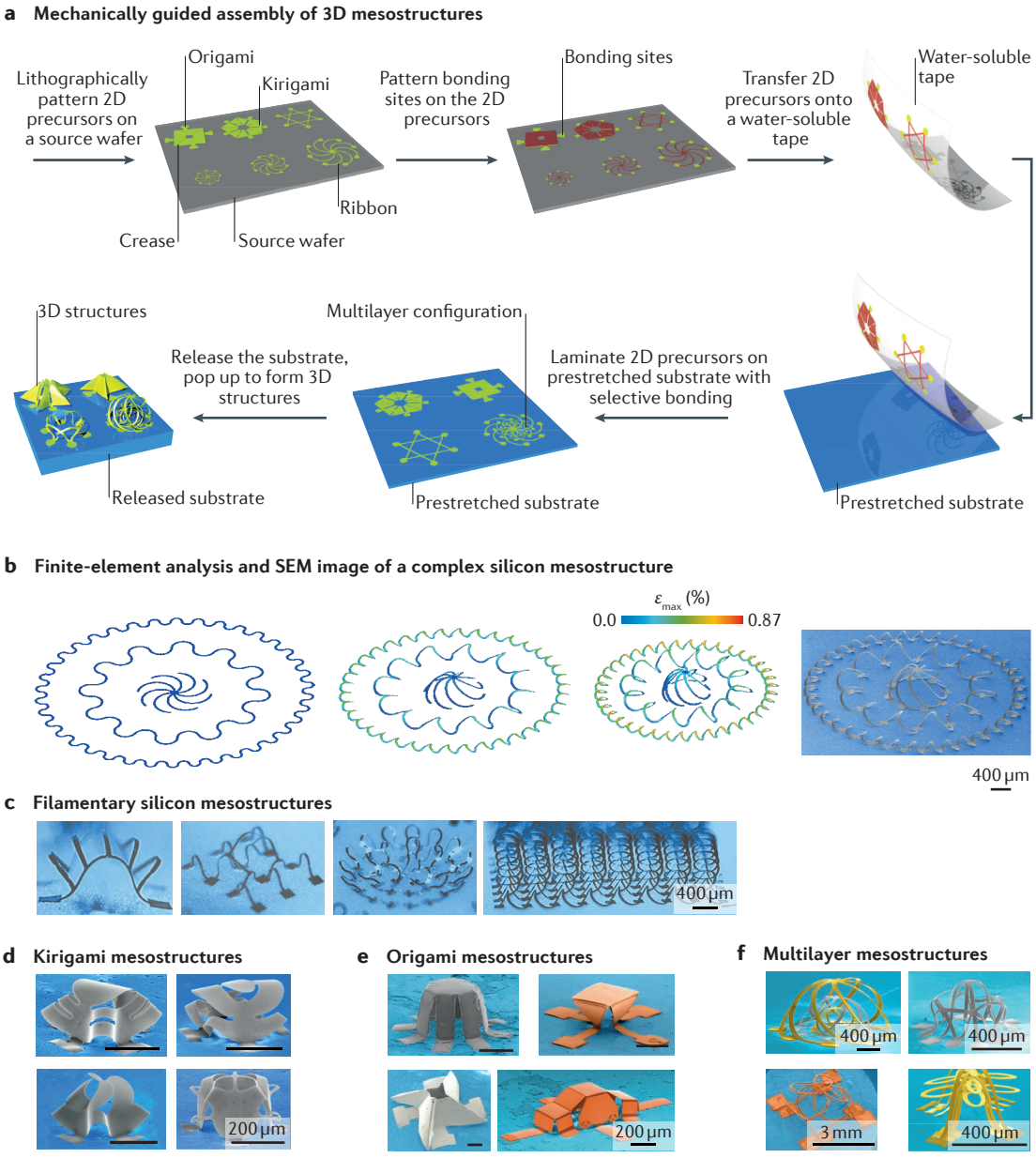

Figure 7 | **Mechanically guided self-assembly: schemes and structures. a** | Schematic illustration of steps for fabricating 3D mesostructures by controlled mechanical buckling of 2D precursors formed using lithographic techniques. **b** | Finite-element analysis results (left three frames) that describe the 2D to 3D geometrical transformation associated with the formation of a complex 3D silicon mesostructure that consists of a concentric pair of toroids and a separate hemispherical 'cage' at the centre, along with a corresponding scanning electron microscope (SEM) image (right) of the final configuration. **c** | Optical images of various 3D filamentary silicon mesostructures. **d** | SEM images of various 3D kirigami mesostructures of silicon and epoxy bilayers. **e** | SEM images of various 3D origami mesostructures with different materials (silicon coloured in grey and metals coloured in orange). **f** | SEM images of various 3D multilayer mesostructures with different materials (epoxy coloured in yellow, silicon coloured in grey and metals coloured in orange). ε_{max}, maximum principal strain. Panels **b** and **c** are adapted with permission from REF. 74, AAAS. Panel **d** is adapted with permission from REF. 93, National Academy of Sciences. Panel **e** is adapted with permission from REF. 95, Wiley-VCH. Panel **f** is adapted with permission from REF. 75, AAAS.

counterparts (FIG. 8d). Rotating micro-mirrors with tilt angles that can be adjusted in a programmable manner for beam steering and modulating the transmission are also possible[93]. The use of active or passive cell scaffolds as 3D frameworks represents an additional area of active exploration.

Further advances will follow from the development of routes to free-standing, isolated 3D mesostructures after separation from the elastomeric substrates. Opportunities also exist in extending these concepts in mechanical assembly from structures with lateral sizes in the nanoscale regime to graphene and other 2D materials.

© 2017 Macmillan Publishers Limited, part of Springer Nature. All rights reserved.

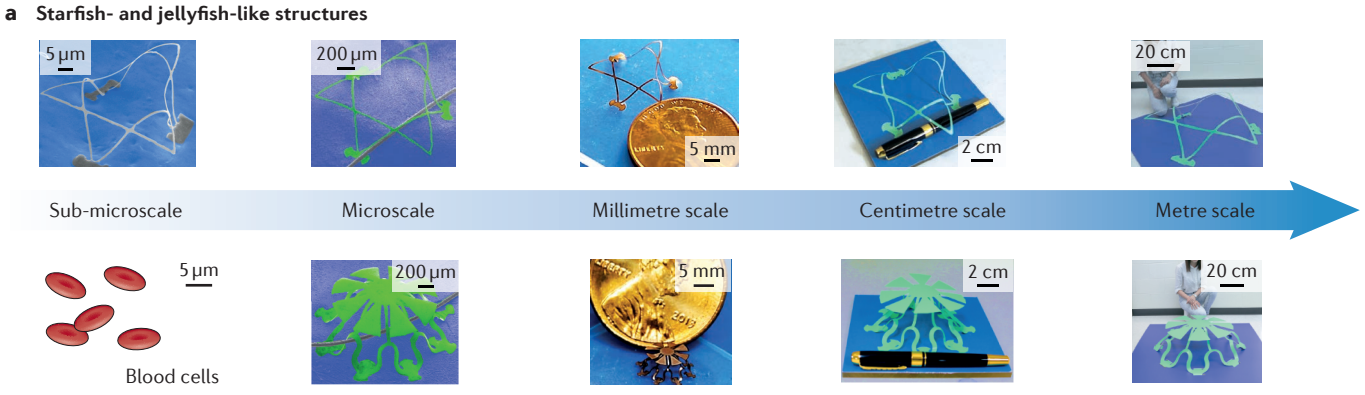

Figure 8 | **Mechanically guided self-assembly: material and size diversity with applications. a** | 3D starfish-like and jellyfish-like structures with characteristic dimensions that span a wide range of length scales. The materials for the sub-micrometre, micrometre, millimetre, centimetre and metre scale structures are silicon, polyimide, bilayers of copper and polyimide, polyester and polyvinyl chloride, respectively. **b** | Experimental images of 3D mesostructures made of metal (Ni and Au), polymer (epoxy (SU8) and polyimide (PI)), and heterogeneous combinations of these materials (SU8–Au and SU8–Si). Scale bars are 200 μm. **c** | Frequency dependence of the inductance and the *Q* factor of a circular inductor mechanically configured into three different shapes. The images are simulation results for the magnetic field (***H***) distributions (feed-in power, 1 W), in which the arrows indicate the direction and their colours indicate the magnitude. **d** | Optical images of a 3D near-field communication device at partial and full release of prestretch in the substrate, and during power supply to a red light-emitting diode. The graph shows the dependence of the *Q* factor on the applied strain for devices with two different widths in the supporting ribbon. Panel **a** is adapted with permission from REF. 202, Elsevier. Panel **b** is adapted with permission from REF. 74, AAAS, and REF. 93, National Academy of Sciences. Panel **c** is adapted with permission from REF. 74, AAAS. Panel **d** is adapted with permission from REF. 75, AAAS.

Conclusion and outlook

Widespread emerging and envisioned applications of 3D micro- and nanostructures — from electronics and photonics, to energy storage and biomedicine — provide strong motivation for the development of new patterning concepts and advanced materials that create designer properties in metamaterials, and engineering design options beyond those of traditional planar systems. Recent progress has established a broad range of techniques with impressive capabilities in forming 3D architectures, in which critical feature sizes can be as small as tens of nanometres or less, and the thicknesses and overall spatial extents can reach centimetres or more. Although the various available methods outlined in this article each offer powerful features, none is without limitations — some in accessible materials, others in realizable geometries and others in throughput and/or feature sizes. For example, TPL and nozzle-based printing

© 2017 Macmillan Publishers Limited, part of Springer Nature. All rights reserved.

techniques offer remarkably high levels of control over 3D geometries, but further advances are needed to allow for rapid processing and use with high-performance materials[148]. Assembly methods inspired by origami and kirigami concepts can operate at high speed, and systematic rules now exist in lattice kirigami methods[203,204] and origami algorithms[205] for folding flat plates into complex targeted 3D configurations. Nevertheless, schemes that avoid requirements for manual intervention, particularly at the micro- and nanoscale, are needed, as are approaches for use with high performance, active materials and advanced planar technologies. Mechanically guided assembly methods do not have such limitations, but the development of design rules for mapping desired 3D structures onto 2D precursors is in its infancy. The ability to combine these various methods together in an integrated approach might facilitate progress towards the ultimate goal of establishing methods that allow for rapid formation of arbitrary 3D architectures in any heterogeneous collection of constituent materials.

Of course, opportunities also exist in the exploration of fundamentally different types of approaches.

Materials science will remain at the core of these activities, but in ways that integrate expertise from the fields of electrical engineering, mechanical engineering, chemical engineering, cell biology, biomedical engineering and others. The foundational research encompasses many topics of fundamental interest in materials processing and heterogeneous integration; buckling, thin-film mechanics and nanomechanics; optics and electromagnetics; polymer science and physics; and adhesion and interface science. The technology pull associated with applications that can benefit from or are enabled by 3D geometries will continue to serve as a strong motivation for further research in this area. Even now, impressive progress outlined in this Review suggests that the question of how to build 3D structures will increasingly shift to what kinds of unique properties in metamaterials and applications in device technologies will follow from the enabled 3D geometries.

1. Pendry, J. B., Holden, A. J., Stewart, W. J. & Youngs, I. Extremely low frequency plasmons in metallic mesostructures. *Phys. Rev. Lett.* **76**, 4773 (1996).
2. Pendry, J. B., Holden, A. J., Robbins, D. J. & Stewart, W. J. Magnetism from conductors and enhanced nonlinear phenomena. *IEEE Trans. Microwave Theory Tech.* **47**, 2075–2084 (1999).
3. Smith, D. R., Padilla, W. J., Vier, D. C., Nemat-Nasser, S. C. & Schultz, S. Composite medium with simultaneously negative permeability and permittivity. *Phys. Rev. Lett.* **84**, 4184 (2000).
4. Shelby, R. A., Smith, D. R. & Schultz, S. Experimental verification of a negative index of refraction. *Science* **292**, 77–79 (2001).
5. Smith, D. R., Pendry, J. B. & Wiltshire, M. C. K. Metamaterials and negative refractive index. *Science* **305**, 788–792 (2004).
6. Shelby, R. A., Smith, D. R., Nemat-Nasser, S. C. & Schultz, S. Microwave transmission through a two-dimensional, isotropic, left-handed metamaterial. *Appl. Phys. Lett.* **78**, 489 (2001).
7. Schurig, D. *et al.* Metamaterial electromagnetic cloak at microwave frequencies. *Science* **314**, 977–980 (2006).
8. Parazzoli, C. G., Greegor, R. B., Li, K., Koltenbah, B. E. C. & Tanielian, M. Experimental verification and simulation of negative index of refraction using Snell's law. *Phys. Rev. Lett.* **90**, 107401 (2003).
9. Linden, S. *et al.* Magnetic response of metamaterials at 100 terahertz. *Science* **306**, 1351–1353 (2004).
10. Yen, T. J. *et al.* Terahertz magnetic response from artificial materials. *Science* **303**, 1494–1496 (2004).
11. Chen, H. T. *et al.* Active terahertz metamaterial devices. *Nature* **444**, 597–600 (2006).
12. Lezec, H. J., Dionne, J. A. & Atwater, H. A. Negative refraction at visible frequencies. *Science* **316**, 430–432 (2007).
13. Zhang, S. *et al.* Experimental demonstration of near-infrared negative-index metamaterials. *Phys. Rev. Lett.* **95**, 137404 (2005).
14. Cai, W. S., Chettiar, U. K., Kildishev, A. V. & Shalaev, V. M. Optical cloaking with metamaterials. *Nat. Photonics* **1**, 224–227 (2007).
15. Liu, N. *et al.* Three-dimensional photonic metamaterials at optical frequencies. *Nat. Mater.* **7**, 31–37 (2008).
16. Valentine, J. *et al.* Three-dimensional optical metamaterial with a negative refractive index. *Nature* **455**, 376–379 (2008).
17. Norris, D. J., Arlinghaus, E. G., Meng, L. L., Heiny, R. & Scriven, L. E. Opaline photonic crystals: how does self-assembly work? *Adv. Mater.* **16**, 1393–1399 (2004).
18. Campbell, M., Sharp, D. N., Harrison, M. T., Denning, R. G. & Turberfield, A. J. Fabrication of photonic crystals for the visible spectrum by holographic lithography. *Nature* **404**, 53–56 (2000).
19. Jeon, S. *et al.* Fabricating complex three-dimensional nanostructures with high-resolution conformable phase masks. *Proc. Natl Acad. Sci. USA* **101**, 12428–12433 (2004).
20. Maldovan, M. & Thomas, E. L. Diamond-structured photonic crystals. *Nat. Mater.* **3**, 593–600 (2004).
21. Jang, J. H. *et al.* 3D micro- and nanostructures via interference lithography. *Adv. Funct. Mater.* **17**, 3027–3041 (2007).
22. Lin, S. Y. *et al.* A three-dimensional photonic crystal operating at infrared wavelengths. *Nature* **394**, 251–253 (1998).
23. Noda, S., Tomoda, K., Yamamoto, N. & Chutinan, A. Full three-dimensional photonic bandgap crystals at near-infrared wavelengths. *Science* **289**, 604–606 (2000).
24. Qi, M. H. *et al.* A three-dimensional optical photonic crystal with designed point defects. *Nature* **429**, 538–542 (2004).
25. Shir, D. *et al.* Three dimensional silicon photonic crystals fabricated by two photon phase mask lithography. *Appl. Phys. Lett.* **94**, 011101 (2009).
26. Cumpston, B. H. *et al.* Two-photon polymerization initiators for three-dimensional optical data storage and microfabrication. *Nature* **398**, 51–54 (1999). **This paper introduces materials and methods for two-photon lithography techniques.**
27. Kawata, S., Sun, H. B., Tanaka, T. & Takada, K. Finer features for functional microdevices: micromachines can be created with higher resolution using two-photon absorption. *Nature* **412**, 697–698 (2001).
28. Deubel, M. *et al.* Direct laser writing of three-dimensional photonic-crystal templates for telecommunications. *Nat. Mater.* **3**, 444–447 (2004).
29. LaFratta, C. N., Fourkas, J. T., Baldacchini, T. & Farrer, R. A. Multiphoton fabrication. *Angew. Chem. Int. Ed.* **46**, 6238–6258 (2007).
30. Gansel, J. K. *et al.* Gold helix photonic metamaterial as broadband circular polarizer. *Science* **325**, 1513–1515 (2009).
31. Ergin, T., Stenger, N., Brenner, P., Pendry, J. B. & Wegener, M. Three-dimensional invisibility cloak at optical wavelengths. *Science* **328**, 337–339 (2010).
32. von Freymann, G. *et al.* Three-dimensional nanostructures for photonics. *Adv. Funct. Mater.* **20**, 1038–1052 (2010).
33. Narayana, S. & Sato, Y. Heat flux manipulation with engineered thermal materials. *Phys. Rev. Lett.* **108**, 214303 (2012).
34. Han, T. C. *et al.* Experimental demonstration of a bilayer thermal cloak. *Phys. Rev. Lett.* **112**, 054302 (2014).
35. Xu, H. Y., Shi, X. H., Gao, F., Sun, H. D. & Zhang, B. L. Ultrathin three-dimensional thermal cloak. *Phys. Rev. Lett.* **112**, 054301 (2014).
36. Liu, Z. Y. *et al.* Locally resonant sonic materials. *Science* **289**, 1734–1736 (2000).
37. Fang, N. *et al.* Ultrasonic metamaterials with negative modulus. *Nat. Mater.* **5**, 452–456 (2006).
38. Hussein, M. I., Leamy, M. J. & Ruzzene, M. Dynamics of phononic materials and structures: historical origins, recent progress, and future outlook. *Appl. Mech. Rev.* **66**, 040802 (2014).
39. Cummer, S. A., Christensen, J. & Alu, A. Controlling sound with acoustic metamaterials. *Nat. Rev. Mater.* **1**, 16001 (2016).
40. Schaedler, T. A. *et al.* Ultralight metallic microlattices. *Science* **334**, 962–965 (2011).
41. Jang, D. C., Meza, L. R., Greer, F. & Greer, J. R. Fabrication and deformation of three-dimensional hollow ceramic nanostructures. *Nat. Mater.* **12**, 893–898 (2013).
42. Meza, L. R., Das, S. & Greer, J. R. Strong, lightweight, and recoverable three-dimensional ceramic nanolattices. *Science* **345**, 1322 (2014).
43. Zheng, X. Y. *et al.* Ultralight, ultrastiff mechanical metamaterials. *Science* **344**, 1373–1377 (2014).
44. Zheng, X. *et al.* Multiscale metallic metamaterials. *Nat. Mater.* **15**, 1100–1106 (2016). **This paper describes improved methods for PμSL formation of metamaterials with hierarchical geometries and diverse feature sizes.**
45. Babaee, S. *et al.* 3D soft metamaterials with negative poisson's ratio. *Adv. Mater.* **25**, 5044–5049 (2013).
46. Coulais, C., Teomy, E., de Reus, K., Shokef, Y. & van Hecke, M. Combinatorial design of textured mechanical metamaterials. *Nature* **535**, 529–532 (2016).
47. Florijn, B., Coulais, C. & van Hecke, M. Programmable mechanical metamaterials. *Phys. Rev. Lett.* **113**, 175503 (2014).
48. Overvelde, J. T. B., Weaver, J. C., Hoberman, C. & Bertoldi, K. Rational design of reconfigurable prismatic architected materials. *Nature* **541**, 347–352 (2017).
49. Wang, Q. *et al.* Lightweight mechanical metamaterials with tunable negative thermal expansion. *Phys. Rev. Lett.* **117**, 175901 (2016).
50. Brunet, T. *et al.* Soft 3D acoustic metamaterial with negative index. *Nat. Mater.* **14**, 384–388 (2015).
51. Brunet, T., Leng, J. & Mondain-Monval, O. Soft acoustic metamaterials. *Science* **342**, 323–324 (2013).

© 2017 Macmillan Publishers Limited, part of Springer Nature. All rights reserved.

52. Raffy, S., Mascaro, B., Brunet, T., Mondain-Monval, O. & Leng, J. A soft 3D acoustic metafluid with dual-band negative refractive index. *Adv. Mater.* **28**, 1760–1764 (2016).
53. Tian, B. Z. *et al.* Macroporous nanowire nanoelectronic scaffolds for synthetic tissues. *Nat. Mater.* **11**, 986–994 (2012).
54. Leong, T. G. *et al.* Tetherless thermobiochemically actuated microgrippers. *Proc. Natl Acad. Sci. USA* **106**, 703–708 (2009).
This paper demonstrates a folding-based method to create 3D microgrippers for biomedical applications.
55. Yu, M. R. *et al.* Semiconductor nanomembrane tubes: three-dimensional confinement for controlled neurite outgrowth. *ACS Nano* **5**, 2447–2457 (2011).
56. Feiner, R. *et al.* Engineered hybrid cardiac patches with multifunctional electronics for online monitoring and regulation of tissue function. *Nat. Mater.* **15**, 679–685 (2016).
57. Froeter, P. *et al.* Toward intelligent synthetic neural circuits: directing and accelerating neuron cell growth by self-rolled-up silicon nitride microtube array. *ACS Nano* **8**, 11108–11117 (2014).
58. Bishop, D., Pardo, F., Bolle, C., Giles, R. & Aksyuk, V. Silicon micro-machines for fun and profit. *J. Low Temp. Phys.* **169**, 386–399 (2012).
59. Wood, R. J. The challenge of manufacturing between macro and micro. *Am. Sci.* **102**, 124–131 (2014).
60. Piyawattanametha, W., Patterson, P. R., Hah, D., Toshiyoshi, H. & Wu, M. C. Surface- and bulk-micromachined two-dimensional scanner driven by angular vertical comb actuators. *J. Microelectromech. Syst.* **14**, 1329–1338 (2005).
61. Zhang, H. G., Yu, X. D. & Braun, P. V. Three-dimensional bicontinuous ultrafast-charge and -discharge bulk battery electrodes. *Nat. Nanotechnol.* **6**, 277 (2011).
62. Pan, L. *et al.* Hierarchical nanostructured conducting polymer hydrogel with high electrochemical activity. *Proc. Natl Acad. Sci. USA* **109**, 9287–9292 (2012).
63. Deng, J. W. *et al.* Naturally rolled-up C/Si/C trilayer nanomembranes as stable anodes for lithium-ion batteries with remarkable cycling performance. *Angew. Chem. Int. Ed.* **52**, 2326–2330 (2013).
64. Wu, H. *et al.* Stable Li-ion battery anodes by *in-situ* polymerization of conducting hydrogel to conformally coat silicon nanoparticles. *Nat. Commun.* **4**, 1943 (2013).
65. Pikul, J. H., Zhang, H. G., Cho, J., Braun, P. V. & King, W. P. High-power lithium ion microbatteries from interdigitated three-dimensional bicontinuous nanoporous electrodes. *Nat. Commun.* **4**, 1732 (2013).
66. Sun, K. *et al.* 3D printing of interdigitated Li-ion microbattery architectures. *Adv. Mater.* **25**, 4539–4543 (2013).
67. Fan, Z. *et al.* Three-dimensional nanopillar-array photovoltaics on low-cost and flexible substrates. *Nat. Mater.* **8**, 648–653 (2009).
68. Lamoureux, A., Lee, K., Shlian, M., Forrest, S. R. & Shtein, M. Dynamic kirigami structures for integrated solar tracking. *Nat. Commun.* **6**, 8092 (2015).
69. Rogers, J., Huang, Y. G., Schmidt, O. G. & Gracias, D. H. Origami MEMS and NEMS. *MRS Bull.* **41**, 123–129 (2016).
70. Ahn, B. Y. *et al.* Omnidirectional printing of flexible, stretchable, and spanning silver microelectrodes. *Science* **323**, 1590–1593 (2009).
This paper introduces a method of nozzle-based 3D printing with conductive inks and presents some examples in free-standing electrical interconnects.
71. Huang, W. *et al.* On-chip inductors with self-rolled-up SiN_x nanomembrane tubes: a novel design platform for extreme miniaturization. *Nano Lett.* **12**, 6283–6288 (2012).
72. Huang, W., Koric, S., Yu, X., Hsia, K. J. & Li, X. L. Precision structural engineering of self-rolled-up 3D nanomembranes guided by transient quasi-static FEM modeling. *Nano Lett.* **14**, 6293–6297 (2014).
73. Grimm, D. *et al.* Rolled-up nanomembranes as compact 3D architectures for field effect transistors and fluidic sensing applications. *Nano Lett.* **13**, 213–218 (2013).
74. Xu, S. *et al.* Assembly of micro/nanomaterials into complex, three-dimensional architectures by compressive buckling. *Science* **347**, 154–159 (2015).
This paper introduces a mechanical assembly approach that allows formation of complex 3D mesostructures from 2D precursors by controlled buckling processes.
75. Yan, Z. *et al.* Mechanical assembly of complex, 3D mesostructures from releasable multilayers of advanced materials. *Sci. Adv.* **2**, e1601014 (2016).
76. Yu, X. *et al.* Ultra-small, high-frequency, and substrate-immune microtube inductors transformed from 2D to 3D. *Sci. Rep.* **5**, 9661 (2015).
77. Januszewicz, R., Tumbleston, J. R., Quintanilla, A. L., Mecham, S. J. & DeSimone, J. M. Layerless fabrication with continuous liquid interface production. *Proc. Natl Acad. Sci. USA* **113**, 11703–11708 (2016).
78. Tumbleston, J. R. *et al.* Continuous liquid interface production of 3D objects. *Science* **347**, 1349–1352 (2015).
This paper introduces continuous liquid interface production techniques for high speed, 3D printing of photopolymerizable resins.
79. Adams, J. J. *et al.* Conformal printing of electrically small antennas on three-dimensional surfaces. *Adv. Mater.* **23**, 1335–1340 (2011).
80. Skylar-Scott, M. A., Gunasekaran, S. & Lewis, J. A. Laser-assisted direct ink writing of planar and 3D metal architectures. *Proc. Natl Acad. Sci. USA* **113**, 6137–6142 (2016).
81. Dickey, M. D. *et al.* Eutectic gallium-indium (EGaIn): a liquid metal alloy for the formation of stable structures in microchannels at room temperature. *Adv. Funct. Mater.* **18**, 1097–1104 (2008).
82. Ladd, C., So, J. H., Muth, J. & Dickey, M. D. 3D printing of free standing liquid metal microstructures. *Adv. Mater.* **25**, 5081–5085 (2013).
83. Parekh, D. P., Ladd, C., Panich, L., Moussa, K. & Dickey, M. D. 3D printing of liquid metals as fugitive inks for fabrication of 3D microfluidic channels. *Lab. Chip* **16**, 1812–1820 (2016).
84. Kong, Y. L. *et al.* 3D printed quantum dot light-emitting diodes. *Nano Lett.* **14**, 7017–7023 (2014).
85. Murphy, S. V. & Atala, A. 3D bioprinting of tissues and organs. *Nat. Biotechnol.* **32**, 773–785 (2014).
86. Konga, Y. L., Guptab, M. K., Johnsonc, B. N. & McAlpined, M. C. 3D printed bionic nanodevices. *Nano Today* **11**, 330–350 (2016).
87. Shenoy, V. B. & Gracias, D. H. Self-folding thin-film materials: from nanopolyhedra to graphene origami. *MRS Bull.* **37**, 847–854 (2012).
88. Leong, T. G., Zarafshar, A. M. & Gracias, D. H. Three-dimensional fabrication at small size scales. *Small* **6**, 792–806 (2010).
89. Py, C. *et al.* Capillary origami: spontaneous wrapping of a droplet with an elastic sheet. *Phys. Rev. Lett.* **98**, 156103 (2007).
90. Guo, X. Y. *et al.* Two- and three-dimensional folding of thin film single-crystalline silicon for photovoltaic power applications. *Proc. Natl Acad. Sci. USA* **106**, 20149–20154 (2009).
91. Mei, Y. F., Solovev, A. A., Sanchez, S. & Schmidt, O. G. Rolled-up nanotech on polymers: from basic perception to self-propelled catalytic microengines. *Chem. Soc. Rev.* **40**, 2109–2119 (2011).
92. Blees, M. K. *et al.* Graphene kirigami. *Nature* **524**, 204–207 (2015).
93. Zhang, Y. H. *et al.* A mechanically driven form of Kirigami as a route to 3D mesostructures in micro/nanomembranes. *Proc. Natl Acad. Sci. USA* **112**, 11757–11764 (2015).
This paper describes kirigami-inspired concepts for the mechanically guided assembly of 3D mesostructures from 2D membrane precursors.
94. Liu, Y. *et al.* Guided formation of 3D helical mesostructures by mechanical buckling: analytical modeling and experimental validation. *Adv. Funct. Mater.* **26**, 2909–2918 (2016).
95. Yan, Z. *et al.* Controlled mechanical buckling for origami-inspired construction of 3D microstructures in advanced materials. *Adv. Funct. Mater.* **26**, 2629–2639 (2016).
96. Shi, Y. *et al.* Plasticity-induced origami for assembly of three dimensional metallic structures guided by compressive buckling. *Extreme Mech. Lett.* **11**, 105–110 (2017).
97. Nan, K. *et al.* Engineered elastomer substrates for guided assembly of complex 3D mesostructures by spatially nonuniform compressive buckling. *Adv. Funct. Mater.* **27**, 1604281 (2017).
98. Lewis, J. A. & Gratson, G. M. Direct writing in three dimensions. *Mater. Today* **7**, 32–39 (2004).
99. Cesarano, J., Segalman, R. & Calvert, P. Robocasting provides moldless fabrication from slurry deposition. *Ceram. Ind.* **148**, 94–102 (1998).
100. Song, J. H., Edirisinghe, M. J. & Evans, J. R. G. Formulation and multilayer jet printing of ceramic inks. *J. Am. Ceram. Soc.* **82**, 3374–3380 (1999).
101. Truby, R. L. & Lewis, J. A. Printing soft matter in three dimensions. *Nature* **540**, 371–378 (2016).
102. Derby, B. Printing and prototyping of tissues and scaffolds. *Science* **338**, 921–926 (2012).
103. Seerden, K. A. M. *et al.* Ink-jet printing of wax-based alumina suspensions. *J. Am. Ceram. Soc.* **84**, 2514–2520 (2001).
104. Wilson, W. C. & Boland, T. Cell and organ printing 1: protein and cell printers. *Anat. Rec. Part A* **272A**, 491–496 (2003).
105. Raney, J. R. & Lewis, J. A. Printing mesoscale architectures. *MRS Bull.* **40**, 943–950 (2015).
106. Lewis, J. A. Direct-write assembly of ceramics from colloidal inks. *Curr. Opin. Solid State Mater. Sci.* **6**, 245–250 (2002).
107. Smay, J. E., Gratson, G. M., Shepherd, R. F., Cesarano, J. & Lewis, J. A. Directed colloidal assembly of 3D periodic structures. *Adv. Mater.* **14**, 1279–1283 (2002).
108. Li, Q. & Lewis, J. A. Nanoparticle inks for directed assembly of three-dimensional periodic structures. *Adv. Mater.* **15**, 1639–1643 (2003).
109. Therriault, D., White, S. R. & Lewis, J. A. Chaotic mixing in three-dimensional microvascular networks fabricated by direct-write assembly. *Nat. Mater.* **2**, 265–271 (2003).
110. Gratson, G. M., Xu, M. J. & Lewis, J. A. Microperiodic structures: direct writing of three-dimensional webs. *Nature* **428**, 386 (2004).
111. Kolesky, D. B., Homan, K. A., Skylar-Scott, M. A. & Lewis, J. A. Three-dimensional bioprinting of thick vascularized tissues. *Proc. Natl Acad. Sci. USA* **113**, 3179–3184 (2016).
112. Duan, B., Hockaday, L. A., Kang, K. H. & Butcher, J. T. 3D Bioprinting of heterogeneous aortic valve conduits with alginate/gelatin hydrogels. *J. Biomed. Mater. Res. A* **101**, 1255–1264 (2013).
113. Duan, B., Kapetanovic, E., Hockaday, L. A. & Butcher, J. T. Three-dimensional printed trileaflet valve conduits using biological hydrogels and human valve interstitial cells. *Acta Biomater.* **10**, 1836–1846 (2014).
114. Hockaday, L. A. *et al.* Rapid 3D printing of anatomically accurate and mechanically heterogeneous aortic valve hydrogel scaffolds. *Biofabrication* **4**, 035005 (2012).
115. Cohen, D. L., Malone, E., Lipson, H. & Bonassar, L. J. Direct freeform fabrication of seeded hydrogels in arbitrary geometries. *Tissue Eng.* **12**, 1325–1335 (2006).
116. Cui, X. F., Breitenkamp, K., Finn, M. G., Lotz, M. & D'Lima, D. D. Direct human cartilage repair using three-dimensional bioprinting technology. *Tissue Eng. Part A* **18**, 1304–1312 (2012).
This paper presents results on inkjet 3D printing of biological materials for direct human cartilage repair.
117. Mannoor, M. S. *et al.* 3D printed bionic ears. *Nano Lett.* **13**, 2634–2639 (2013).
118. De Coppi, P. *et al.* Isolation of amniotic stem cell lines with potential for therapy. *Nat. Biotechnol.* **25**, 100–106 (2007).
119. Jakus, A. E. *et al.* Hyperelastic "bone": a highly versatile, growth factor–free, osteoregenerative, scalable, and surgically friendly biomaterial. *Sci. Transl. Med.* **8**, 358ra127 (2016).
This paper describes classes of synthetic osteoregenerative biomaterials for 3D bioprinting of versatile, hyperelastic 'bone' constructs.
120. Rutz, A. L., Hyland, K. E., Jakus, A. E., Burghardt, W. R. & Shah, R. N. A multimaterial bioink method for 3D printing tunable, cell-compatible hydrogels. *Adv. Mater.* **27**, 1607–1614 (2015).
121. Kolesky, D. B. *et al.* 3D bioprinting of vascularized, heterogeneous cell-laden tissue constructs. *Adv. Mater.* **26**, 3124–3130 (2014).
This paper demonstrates multimaterial 3D printing of vascularized tissue structures with disparate chemical and mechanical properties.
122. Johnson, B. N. *et al.* 3D printed nervous system on a chip. *Lab. Chip* **16**, 1393–1400 (2016).

© 2017 Macmillan Publishers Limited, part of Springer Nature. All rights reserved.

123. Skardal, A. *et al.* Bioprinted amniotic fluid-derived stem cells accelerate healing of large skin wounds. *Stem Cells Transl. Med.* **1**, 792–802 (2012).
124. Johnson, B. N. *et al.* 3D printed anatomical nerve regeneration pathways. *Adv. Funct. Mater.* **25**, 6205–6217 (2015).
125. Xu, T. *et al.* Hybrid printing of mechanically and biologically improved constructs for cartilage tissue engineering applications. *Biofabrication* **5**, 015001 (2013).
126. Maruo, S., Nakamura, O. & Kawata, S. Three-dimensional microfabrication with two-photon-absorbed photopolymerization. *Opt. Lett.* **22**, 132–134 (1997).
127. Maruo, S. & Kawata, S. Two-photon-absorbed near-infrared photopolymerization for three-dimensional microfabrication. *J. Microelectromech. Syst.* **7**, 411–415 (1998).
128. Sun, H. B. *et al.* Real three-dimensional microstructures fabricated by photopolymerization of resins through two-photon absorption. *Opt. Lett.* **25**, 1110–1112 (2000).
129. Zhang, X., Jiang, X. N. & Sun, C. Micro-stereolithography of polymeric and ceramic microstructures. *Sens. Actuators A* **77**, 149–156 (1999).
130. Hull, C. *et al.* Rapid prototyping: current technology and future potential. *Rapid Prototyp. J.* **1**, 11–19 (1995).
131. Sun, C., Fang, N., Wu, D. M. & Zhang, X. Projection micro-stereolithography using digital micro-mirror dynamic mask. *Sens. Actuators A* **121**, 113–120 (2005).
This paper describes methods for PμSL as routes to high-speed printing of complex 3D microstructures.
132. Kumar, S. Selective laser sintering: a qualitative and objective approach. *JOM* **55**, 43–47 (2003).
133. Zheng, X. Y. *et al.* Design and optimization of a light-emitting diode projection micro-stereolithography three-dimensional manufacturing system. *Rev. Sci. Instrum.* **83**, 125001 (2012).
134. Johnson, A. R. *et al.* Single-step fabrication of computationally designed microneedles by continuous liquid interface production. *PLoS ONE* **11**, e0162518 (2016).
135. Maruo, S. & Fourkas, J. T. Recent progress in multiphoton microfabrication. *Laser Photonics Rev.* **2**, 100–111 (2008).
136. Liu, Y. M. & Zhang, X. Metamaterials: a new frontier of science and technology. *Chem. Soc. Rev.* **40**, 2494–2507 (2011).
137. Soukoulis, C. M. & Wegener, M. Past achievements and future challenges in the development of three-dimensional photonic metamaterials. *Nat. Photonics* **5**, 523–530 (2011).
138. Zheludev, N. I. & Kivshar, Y. S. From metamaterials to metadevices. *Nat. Mater.* **11**, 917–924 (2012).
139. Galajda, P. & Ormos, P. Complex micromachines produced and driven by light. *Appl. Phys. Lett.* **78**, 249–251 (2001).
140. Galajda, P. & Ormos, P. Rotors produced and driven in laser tweezers with reversed direction of rotation. *Appl. Phys. Lett.* **80**, 4653–4655 (2002).
141. Maruo, S., Ikuta, K. & Korogi, H. Submicron manipulation tools driven by light in a liquid. *Appl. Phys. Lett.* **82**, 133–135 (2003).
142. Maruo, S. & Inoue, H. Optically driven micropump produced by three-dimensional two-photon microfabrication. *Appl. Phys. Lett.* **89**, 144101 (2006).
143. Wu, P. W. *et al.* Two-photon photographic production of three-dimensional metallic structures within a dielectric matrix. *Adv. Mater.* **12**, 1438–1441 (2000).
144. Stellacci, F. *et al.* Laser and electron-beam induced growth of nanoparticles for 2D and 3D metal patterning. *Adv. Mater.* **14**, 194–198 (2002).
145. Baldacchini, T. *et al.* Multiphoton laser direct writing of two-dimensional silver structures. *Opt. Express* **13**, 1275–1280 (2005).
146. Tanaka, T., Ishikawa, A. & Kawata, S. Two-photon-induced reduction of metal ions for fabricating three-dimensional electrically conductive metallic microstructure. *Appl. Phys. Lett.* **88**, 081107 (2006).
147. Meza, L. R. *et al.* Resilient 3D hierarchical architected metamaterials. *Proc. Natl Acad. Sci. USA* **112**, 11502–11507 (2015).
148. Montemayor, L., Chernow, V. & Greer, J. R. Materials by design: using architecture in material design to reach new property spaces. *MRS Bull.* **40**, 1122–1129 (2015).
149. Xu, C., Gallant, B. M., Wunderlich, P. U., Lohmann, T. & Greer, J. R. Three-dimensional Au microlattices as positive electrodes for Li–O_2 batteries. *ACS Nano* **9**, 5876–5883 (2015).
150. Bauer, J., Hengsbach, S., Tesari, I., Schwaiger, R. & Kraft, O. High-strength cellular ceramic composites with 3D microarchitecture. *Proc. Natl Acad. Sci. USA* **111**, 2453–2458 (2014).
151. Meza, L. R. & Greer, J. R. Mechanical characterization of hollow ceramic nanolattices. *J. Mater. Sci.* **49**, 2496–2508 (2014).
152. Montemayor, L. C. & Greer, J. R. Mechanical response of hollow metallic nanolattices: combining structural and material size effects. *J. Appl. Mech.* **82**, 071012 (2015).
153. Gladman, A. S., Matsumoto, E. A., Nuzzo, R. G., Mahadevan, L. & Lewis, J. A. Biomimetic 4D printing. *Nat. Mater.* **15**, 413–418 (2016).
This paper describes a biomimetic hydrogel composite for programmable 4D printing.
154. Tibbits, S. 4D printing: multi-material shape change. *Archit. Design* **84**, 116–121 (2014).
155. Raviv, D. *et al.* Active printed materials for complex self-evolving deformations. *Sci. Rep.* **4**, 7422 (2014).
156. Ge, Q., Qi, H. J. & Dunn, M. L. Active materials by four-dimension printing. *Appl. Phys. Lett.* **103**, 131901 (2013).
This paper describes 4D printing by use of SMP materials.
157. Ge, Q., Dunn, C. K., Qi, H. J. & Dunn, M. L. Active origami by 4D printing. *Smart Mater. Struct.* **23**, 094007 (2014).
158. Wu, J. T. *et al.* Multi-shape active composites by 3D printing of digital shape memory polymers. *Sci. Rep.* **6**, 24224 (2016).
159. Liu, Y., Genzer, J. & Dickey, M. D. "2D or not 2D": shape-programming polymer sheets. *Prog. Polym. Sci.* **52**, 79–106 (2016).
160. Kang, S. H. & Dickey, M. D. Patterning via self-organization and self-folding: beyond conventional lithography. *MRS Bull.* **41**, 93–96 (2016).
161. Huang, G. S. & Mei, Y. F. Thinning and shaping solid films into functional and integrative nanomembranes. *Adv. Mater.* **24**, 2517–2546 (2012).
162. Chen, Z., Huang, G. S., Trase, I., Han, X. M. & Mei, Y. F. Mechanical self-assembly of a strain-engineered flexible layer: wrinkling, rolling, and twisting. *Phys. Rev. Appl.* **5**, 017001 (2016).
163. Syms, R. R. A. & Yeatman, E. M. Self-assembly of three-dimensional microstructures using rotation by surface tension forces. *Electron. Lett.* **29**, 662–664 (1993).
164. Syms, R. R. A. Equilibrium of hinged and hingeless structures rotated using surface tension forces. *J. Microelectromech. Syst.* **4**, 177–184 (1995).
165. Syms, R. R. A., Yeatman, E. M., Bright, V. M. & Whitesides, G. M. Surface tension-powered self-assembly of microstructures — the state-of-the-art. *J. Microelectromech. Syst.* **12**, 387–417 (2003).
166. Gracias, D. H., Kavthekar, V., Love, J. C., Paul, K. E. & Whitesides, G. M. Fabrication of micrometer-scale, patterned polyhedra by self-assembly. *Adv. Mater.* **14**, 235–238 (2002).
167. Cho, J.-H. *et al.* Nanoscale origami for 3D optics. *Small* **7**, 1943–1948 (2011).
168. Pandey, S. *et al.* Algorithmic design of self-folding polyhedra. *Proc. Natl Acad. Sci. USA* **108**, 19885–19890 (2011).
169. Prinz, V. Y. *et al.* Free-standing and overgrown InGaAs/GaAs nanotubes, nanohelices and their arrays. *Phys. E* **6**, 828–831 (2000).
170. Schmidt, O. G. & Eberl, K. Nanotechnology: thin solid films roll up into nanotubes. *Nature* **410**, 168 (2001).
This paper describes approaches in stress-controlled rolling to form cylindrical 3D nanostructures.
171. Li, X. Strain induced semiconductor nanotubes: from formation process to device applications. *J. Phys. D Appl. Phys.* **41**, 193001 (2008).
172. Li, X. Self-rolled-up microtube ring resonators: a review of geometrical and resonant properties. *Adv. Opt. Photonics* **3**, 366–387 (2011).
173. Prinz, V. Y., Seleznev, V., Samoylov, V. & Gutakovsky, A. Nanoscale engineering using controllable formation of ultra-thin cracks in heterostructures. *Microelectron. Eng.* **30**, 439–442 (1996).
174. Bassik, N., Stern, G. M., Jamal, M. & Gracias, D. H. Patterning thin film mechanical properties to drive assembly of complex 3D structures. *Adv. Mater.* **20**, 4760–4764 (2008).
175. Karnaushenko, D. D., Karnaushenko, D., Makarov, D. & Schmidt, O. G. Compact helical antenna for smart implant applications. *NPG Asia Mater.* **7**, e188 (2015).
176. Mei, Y. *et al.* Versatile approach for integrative and functionalized tubes by strain engineering of nanomembranes on polymers. *Adv. Mater.* **20**, 4085–4090 (2008).
177. Bassik, N., Stern, G. M. & Gracias, D. H. Microassembly based on hands free origami with bidirectional curvature. *Appl. Phys. Lett.* **95**, 091901 (2009).
178. Malachowski, K. *et al.* Self-folding single cell grippers. *Nano Lett.* **14**, 4164–4170 (2014).
179. Solovev, A. A., Mei, Y., Urena, E. B., Huang, G. & Schmidt, O. G. Catalytic microtubular jet engines self-propelled by accumulated gas bubbles. *Small* **5**, 1688–1692 (2009).
180. Wang, H. *et al.* Self-rolling and light-trapping in flexible quantum well-embedded nanomembranes for wide-angle infrared photodetectors. *Sci. Adv.* **2**, e1600027 (2016).
181. Klein, Y., Efrati, E. & Sharon, E. Shaping of elastic sheets by prescription of non-Euclidean metrics. *Science* **315**, 1116–1120 (2007).
182. Kim, J., Hanna, J. A., Byun, M., Santangelo, C. D. & Hayward, R. C. Designing responsive buckled surfaces by halftone gel lithography. *Science* **335**, 1201–1205 (2012).
This paper describes a method of halftone gel lithography to create spatially varying 2D patterns of swelling in gel sheets for transformation into desired 3D shapes.
183. Na, J.-H. *et al.* Programming reversibly self-folding origami with micropatterned photo-crosslinkable polymer trilayers. *Adv. Mater.* **27**, 79–85 (2015).
184. Na, J.-H., Bende, N. P., Bae, J., Santangelo, C. D. & Hayward, R. C. Grayscale gel lithography for programmed buckling of non-Euclidean hydrogel plates. *Soft Matter* **12**, 4985–4990 (2016).
185. Palleau, E., Morales, D., Dickey, M. D. & Velev, O. D. Reversible patterning and actuation of hydrogels by electrically assisted ionoprinting. *Nat. Commun.* **4**, 2257 (2013).
186. Wu, Z. L. *et al.* Three-dimensional shape transformations of hydrogel sheets induced by small-scale modulation of internal stresses. *Nat. Commun.* **4**, 1586 (2013).
187. Hawkes, E. *et al.* Programmable matter by folding. *Proc. Natl Acad. Sci. USA* **107**, 12441–12445 (2010).
188. Liu, Y., Boyles, J. K., Genzer, J. & Dickey, M. D. Self-folding of polymer sheets using local light absorption. *Soft Matter* **8**, 1764–1769 (2012).
189. Felton, S., Tolley, M., Demaine, E., Rus, D. & Wood, R. A method for building self-folding machines. *Science* **345**, 644–646 (2014).
190. Ware, T. H., McConney, M. E., Wie, J. J., Tondiglia, V. P. & White, T. J. Voxelated liquid crystal elastomers. *Science* **347**, 982–984 (2015).
191. White, T. J. & Broer, D. J. Programmable and adaptive mechanics with liquid crystal polymer networks and elastomers. *Nat. Mater.* **14**, 1087–1098 (2015).
192. Jamal, M., Zarafshar, A. M. & Gracias, D. H. Differentially photo-crosslinked polymers enable self-assembling microfluidics. *Nat. Commun.* **2**, 527 (2011).
193. Ryu, J. *et al.* Photo-origami—bending and folding polymers with light. *Appl. Phys. Lett.* **100**, 161908 (2012).
194. Yu, X., Arbabi, E., Goddard, L. L., Li, X. & Chen, X. Monolithically integrated self-rolled-up microtube-based vertical coupler for three-dimensional photonic integration. *Appl. Phys. Lett.* **107**, 031102 (2015).
195. Annett, J. & Cross, G. L. Self-assembly of graphene ribbons by spontaneous self-tearing and peeling from a substrate. *Nature* **535**, 271–275 (2016).
196. Zhu, S. & Li, T. Hydrogenation enabled scrolling of graphene. *J. Phys. D Appl. Phys.* **46**, 075301 (2013).
197. Zhu, S. & Li, T. Hydrogenation-assisted graphene origami and its application in programmable molecular mass uptake, storage, and release. *ACS Nano* **8**, 2864–2872 (2014).
198. Qi, Z. N., Campbell, D. K. & Park, H. S. Atomistic simulations of tension-induced large deformation and stretchability in graphene kirigami. *Phys. Rev. B* **90**, 245437 (2014).

© 2017 Macmillan Publishers Limited, part of Springer Nature. All rights reserved.

199. Grosso, B. F. & Mele, E. J. Bending rules in graphene kirigami. *Phys. Rev. Lett.* **115**, 195501 (2015).
200. Bahamon, D. A., Qi, Z. N., Park, H. S., Pereira, V. M. & Campbell, D. K. Graphene kirigami as a platform for stretchable and tunable quantum dot arrays. *Phys. Rev. B* **93**, 235408 (2016).
201. Patra, N., Wang, B. & Král, P. Nanodroplet activated and guided folding of graphene nanostructures. *Nano Lett.* **9**, 3766–3771 (2009).
202. Yan, Z. *et al.* Deterministic assembly of 3D mesostructures in advanced materials via compressive buckling: a short review of recent progress. *Extreme Mech. Lett.* **11**, 96–104 (2017).
203. Castle, T. *et al.* Making the cut: lattice *kirigami* rules. *Phys. Rev. Lett.* **113**, 245502 (2014).
204. Sussman, D. M. *et al.* Algorithmic lattice kirigami: a route to pluripotent materials. *Proc. Natl Acad. Sci. USA* **112**, 7449–7453 (2015).
205. Dudte, L. H., Vouga, E., Tachi, T. & Mahadevan, L. Programming curvature using origami tessellations. *Nat. Mater.* **15**, 583–588 (2016).

Acknowledgements
J.A.R. and X.L. acknowledge support from the US Department of Energy, Office of Science, Basic Energy Sciences (DE-FG02-07ER46471). Y.Z. acknowledges support from the National Natural Science Foundation of China (11672152) and Thousand Young Talents Program of China. Y.H. acknowledges support from the National Science Foundation (NSF) (CMMI1300846 and CMMI1534120). Y.H. and J.A.R. acknowledge support from the NSF (CMMI1400169) and the National Institutes of Health (R01EB019337).

Competing interests statement
The authors declare no competing interests.

Publisher's note
Springer Nature remains neutral with regard to jurisdictional claims in published maps and institutional affiliations.

How to cite this article
Zhang, Y. *et al*. Printing, folding and assembly methods for forming 3D mesostructures in advanced materials. *Nat. Rev. Mater*. **2**, 17019 (2017).

© 2017 Macmillan Publishers Limited, part of Springer Nature. All rights reserved.

Subject terms
Physical sciences / Materials science / Techniques and instrumentation [URI /639/301/930]
Physical sciences / Materials science / Materials for devices [URI /639/301/1005]
Physical sciences / Materials science / Structural materials [URI /639/301/1023]

Web summary

000 **Printing, folding and assembly methods for forming 3D mesostructures in advanced materials**

Yihui Zhang, Fan Zhang, Zheng Yan, Qiang Ma, Xiuling Li, Yonggang Huang and John A. Rogers

Emerging materials and methods for fabricating 3D micro- and nanostructures provide powerful capabilities of relevance across diverse areas of technology. This Review highlights the latest results and future trends associated with the most powerful methods in 3D printing, folding and assembly.

Figure permissions

Figure 1
Panel **b** is **adapted with permission from** REF. 70, AAAS. Panel **c** is adapted with permission from REF. 79, Wiley-VCH. Panel **d** is adapted with permission from REF. 80, National Academy of Sciences. Panel **e** is adapted with permission from REF. 82, Wiley-VCH. Panel **f** is adapted with permission from REF. 84, American Chemical Society.

Figure 2
Panel **a** is **adapted with permission from** REF. 113, Elsevier. Panel **b** is adapted with permission from REF. 117, American Chemical Society. Panel **c** is adapted with permission from REF. 122, Royal Society of Chemistry. Panel **d** is adapted with permission from REF. 118, Macmillan Publishers Limited. Panel **e** is adapted with permission from REF. 119, AAAS. Panel **f** is adapted with permission from REF. 111, National Academy of Sciences. Panel **g** is adapted with permission from REF. 123, AlphaMed Press. Panel **h** is adapted with permission from REF. 124, Wiley-VCH.

Figure 3
Panels **a** (middle **and right) are adapted with permission from** REF. 42, AAAS. Panel **b** is adapted with permission from REF. 44, Macmillan Publishers Limited. Panel **c** is adapted with permission from REF. 78, AAAS.

Figure 4
Panel **a** is **adapted with permission from** REF. 153, Macmillan Publishers Limited, and REF. 156, AIP Publishing. Panel **b** (top) is adapted with permission from REF. 153, Macmillan Publishers Limited. Panel **b** (bottom) is adapted with permission from REF. 158, Macmillan Publishers Limited.

Figure 5
Panel **b** (four **images, left) is adapted with permission from** REF. 168, National Academy of Sciences. Panel **b** (two images, right) is adapted with permission from REF. 89, American Physical Society. Panel **c** is adapted with permission from REF. 169, Elsevier; REF. 170, Macmillan Publishers Limited; and REF. 176, Wiley-VCH. Panel **d** is adapted with permission from REF. 182, AAAS; REF. 183, Wiley; and REF. 192, Macmillan Publishers Limited.

Figure 6
Panels **a** and **b are adapted with permission from** REF. 92, Macmillan Publishers Limited. Panel **c** is adapted with permission from REF. 195, Macmillan Publishers Limited.

Figure 7
Panels **b** and **c are adapted with permission from** REF. 74, AAAS. Panel **d** is adapted with permission from REF. 93, National Academy of Sciences. Panel **e** is adapted with permission from REF. 95, Wiley. Panel **f** is adapted with permission from REF. 75, AAAS.

Figure 8
Panel **a** is **adapted with permission from** REF. 202, Elsevier. Panel **b** is adapted with permission from REF. 74, AAAS, and REF. 93, National Academy of Sciences. Panel **c** is adapted with permission from REF. 74, AAAS. Panel **d** is adapted with permission from REF. 75, AAAS.

© 2017 Macmillan Publishers Limited, part of Springer Nature. All rights reserved.